A SPECTROSCOPIC STUDY OF THE STELLAR CONTENT OF ELLIPTICAL GALAXIES

by

Elliott Paul Moore

A Dissertation Submitted to the Faculty of the

DEPARTMENT OF ASTRONOMY

In Partial Fulfillment of the Requirements
For the Degree of

DOCTOR OF PHILOSOPHY

In the Graduate College

THE UNIVERSITY OF ARIZONA

1968

THE UNIVERSITY OF ARIZONA

GRADUATE COLLEGE

I hereby recommend that this dissertation prepared under my direction by Elliott Paul Moore

entitled A Spectroscopic Study of the Stellar Content of Elliptical Galaxies

be accepted as fulfilling the dissertation requirement of the degree of Doctor of Philosophy

William G. Tifft — Oct 2, 1967

Dissertation Director — Date

After inspection of the final copy of the dissertation, the following members of the Final Examination Committee concur in its approval and recommend its acceptance:*

[signature]	Oct 2, 1967
[signature]	Oct 2, 1967
Robert E. Williams	Oct. 2, 1967
[signature]	Oct. 2, 1967
[signature]	Oct 3, 1967

*This approval and acceptance is contingent on the candidate's adequate performance and defense of this dissertation at the final oral examination. The inclusion of this sheet bound into the library copy of the dissertation is evidence of satisfactory performance at the final examination.

STATEMENT BY AUTHOR

This dissertation has been submitted in partial fulfillment of requirements for an advanced degree at the University of Arizona and is deposited in the University Library to be made available to borrowers under rules of the Library.

Brief quotations from this dissertation are allowable without special permission, provided that accurate acknowledgment of source is made. Requests for permission for extended quotation from or reproduction of this manuscript in whole or in part may be granted by the copyright holder.

SIGNED: Elliott Moore

TABLE OF CONTENTS

	Page
List of Tables	v
List of Illustrations	vii
Abstract	ix
Statement of Problem	1
Theoretical Considerations	13
Observations	32
Conclusions	39
Appendix I—Observations and Reduction Procedures	53
Appendix II—Theoretical Results and Statistical Tabulations	70
List of References	79

LIST OF TABLES

Table		Page
1	Ratio at M0 V of $\psi(M_V)$ at n/ $\psi(M_V)$ at n = -1.35	19
2	$\psi(M_V)$ as a Function of n	20
3	NGC 188 and Main Sequence Correspondence	26
4	M67 and Main Sequence Correspondence	27
5	Galaxy Properties	33
6	Stellar Observational Data	57
7	Galaxy Observational Data	61
8	M67 Model Results	71
9	M67+M Model Results	72
10	NGC 188 Model Results	73
11	NGC 188+M Model Results	74
12	M67 Observational Average Deviation (AD) and Root Mean Square Error (RMSE)	75
13	M67+M Observational Average Deviation (AD) and Root Mean Square Error (RMSE)	76

LIST OF TABLES---Continued

Table		Page
14	NGC 188 Observational Average Deviation (AD) and Root Mean Square Error (RMSE)	77
15	NGC 188 + M Observational Average Deviation (AD) and Root Mean Square Error (RMSE)	78
16	Comparison of RMSE and Internal Standard Deviation	51

LIST OF ILLUSTRATIONS

Figure		Page
1	Equivalent Widths (Å) vs. B-V for λ 4226	37
2	NGC 221, AD and RMSE vs. n	41
3	NGC 3115, AD and RMSE vs. n	42
4	NGC 3379, AD and RMSE vs. n	43
5	NGC 4472, AD and RMSE vs. n	44
6	Calculated and Observed Equivalent Widths (Å) vs. n for λ 4200 and λ 4226	48
7	M/L vs. n for M67, M67+M, NGC 188, and NGC 188+M	50
8	Stellar and Galaxy Spectra with λ 4404 Tracing	56
9	Equivalent Widths (Å) vs. B-V for λ 4077 and λ 4101	62
10	Equivalent Widths (Å) vs. B-V for λ 4130 and λ 4175	63
11	Equivalent Widths (Å) vs. B-V for λ 4200	64
12	Equivalent Widths (Å) vs. B-V for λ 4226	65
13	Equivalent Widths (Å) vs. B-V for λ 4254 and λ 4275	66

LIST OF ILLUSTRATIONS---Continued

Figure		Page
14	Equivalent Widths (Å) vs. B-V for λ 4289 and λ 4300	67
15	Equivalent Widths (Å) vs. B-V for λ 4340	68
16	Equivalent Widths (Å) vs. B-V for λ 4385 and λ 4404	69

ABSTRACT

Models of the stellar content of the nuclei of elliptical galaxies are constructed to find the range of initial luminosity function and age consistent with observations. The assumptions include: (1) only a single generation of stars exists, (2) the initial mass function and initial luminosity function are approximated by a power law with variable exponent, and (3) color magnitude diagrams at two ages can be based on the old metal-rich clusters NGC 188 and M67. Mass to light ratios and equivalent widths of thirteen spectral features are synthesized for each choice of initial luminosity function and one of two ages.

A comparison of results from the models is made with observations of the ellipticals NGC 221, 3379, 4472 and of the S0 NGC 3115. The basic conclusions are: (1) the initial luminosity function deduced from observations of our galaxy satisfactorily represents the equivalent widths of spectral features in elliptical galaxies. Dwarf enrichment is not likely for all four galaxies, but dwarf depletion may occur in the nuclei of the intermediate mass NGC 3379 and giant NGC 4472.

M/L ratios support the depletion hypothesis. (2) the light in all four galaxies appears to arise from aggregates younger than NGC 188, the oldest known cluster in our galaxy. Three of the four galaxies are well represented by light from a cluster like M67 augmented by M giants; the S0 NGC 3115 appears to require a younger model.

STATEMENT OF PROBLEM

Since the discovery that galaxies are extremely distant groups of stars, astronomers have been interested in determining what kinds of stars are present. This interest arises not from just the challenge as a difficult problem, but because of the usefulness of the answers in a variety of investigations. The determination of the temperatures and luminosities of the stars may yield considerable information about how much time has passed since the stars were formed, and the relative numbers in each temperature and luminosity class may be clues to the physical conditions at that time. The determination of the number of stars as a function of mass is a necessity for many dynamical calculations. The radiation field that the stars form is of importance in the study of gas present in galaxies. The determination of the present luminosity function in elliptical galaxies, and the deduction of what it has been in the past, is of considerable importance in cosmology as the evolutionary correction. Thus, determination of the stellar content of elliptical galaxies is important not only as an end in itself but the beginning of many other investigations.

Observations of elliptical galaxies should be directed also to basic unsolved physical problems; among these problems are the form of the initial mass function and its modification into the observed mass function by evolutionary aging and other processes. This study attempts to determine the range of age and initial mass function in elliptical galaxies which is consistent with observations of mass to light ratios and equivalent widths. Equivalent widths of spectral features are chosen as observational criteria because of: (1) their strong dependence on stellar temperature, luminosity, and chemical composition, (2) their almost complete independence of interstellar reddening by dust in our galaxy and the galaxy observed, and (3) the fact that few quantitative observations of this type have been made of elliptical galaxies.

The first section is a discussion of the present knowledge of stellar composition of ellipticals and Sb spirals, whose nuclei resemble ellipticals in color and spectrum. Then the concept and assumptions of modeling are introduced. The approach is to assume a form for the initial mass spectrum, with a variable parameter that changes the relative numbers of stars of different masses; as this configuration of stars ages, the distribution of stars changes in the color magnitude diagram. The relative numbers of stars in each portion of the color magnitude diagram are

calculated, but the method of calculation restricts the range of an age parameter to the two ages of the old galactic clusters NGC 188 and M67. Each distribution of relative numbers of stars in a color magnitude diagram at a given age and assumed initial mass spectrum is called a model; each model is used to predict equivalent widths and mass to light ratios for comparison with observations of four galaxies. Conclusions are drawn as to which initial mass spectrum and age best fits the observations.

Previous studies of stellar composition of the nuclei of ellipticals and Sb spirals generally agree that an old stellar population is the dominant contributor to the light. Baade (1944) reports that resolution of the brightest stars in the nearest elliptical, the dwarf M32, shows no appreciable number of bright blue main sequence stars; red stars near $M_V = -3$ are resolved before main sequence stars. Morgan and Mayall (1957) use qualitative visual classification of spectra of ellipticals and of M31 to conclude that the earliest contributors are of spectral type F8 with the greatest contributions from late G, K, and M stars. Tifft (1961, 1963) makes eight color photoelectric observations of elliptical and S0 galaxies. He synthesizes colors from an assembly which includes the old Population I cluster M67, an average globular cluster, and stars of types M2 Ia, M2 III,

G2 III, A9 III, and O9 V. He finds a good fit to his galaxy observations with old Population I plus M2 III stars, though somewhat redder stars are also required to match red observations. Studies by Limber (1960) and Spinrad (1962) presented later in this section have as one alternative a population of greater age than any known in our galaxy.

There is rather general agreement that the stars contributing most of the light from the nuclei of ellipticals and Sb spirals are metal-rich stars. Baade's (1944) resolution of the brightest red stars in M32 and the nucleus of M31 near absolute magnitude -3 indicates a metal-poor component similar to the red giant branch of globular clusters. However, Baum's (1959b) investigation of the count/brightness ratio in M31 indicates that the relative proportion of the numbers of such giants is closer to that in the solar neighborhood than in a globular cluster; Baum's calculations show that if all the brightness of the nucleus of M31 were to be produced by stars like those in globulars the count would be 500 images per square millimeter on the plates used, too many to be resolved.

Using qualitative visual classification of integrated spectra, Morgan (1959) states that the spectra of virtually all giant galaxies studied is of the "strong metallic line" variety,

with elemental abundances of the stars within them very similar to the sun. Van den Bergh and Henry (1962) make photoelectric spectral scans of standard stars, M32 and M31, and globular clusters with 35Å resolution of a metal index suggested by Morgan. They conclude that the metal index in the two galaxies is close to the metal-rich stars and quite different from the most metal-rich globular clusters examined; they caution that very late type stars may be influencing the composite metal index, however. Baum (1959a, 1959b) synthesizes a model to fit the sox color observations of Stebbins and Whitford (1948) starting with both metal-rich and metal-poor populations. His metal-rich population is based on M67, broken into K5 giants, G subgiants, G dwarfs, K5 dwarfs, and M0 dwarfs with early M giants and 1900°K components added; his metal-poor population is constructed from globular cluster giant and horizontal branches with dwarf G0, K1, K5 and M0 segments. Baum varies the relative number of stars in each group to find the best fit to the six color measures; his final model closely resembles M67, with only 20% of the visual light from a metal-poor population. Tifft (1963) also finds an old metal-rich population dominates the metal-poor population in his color synthesis.

No general agreement appears to exist on the form of the initial luminosity function. The controversy, frequently

simplified to a discussion of dwarf to giant ratio, appears to have persisted for more than 30 years, and includes discussions of spectra, colors, and mass to light (M/L) ratios. An early paper by Hubble and Humason (1931) states that a few high dispersion spectra of M32 and M31 on blue sensitive plates show dwarf characteristics; no details are given of the criteria used. Öhman (1934) classifies a single red spectrum of the elliptical M32 as dwarflike, due to the absence of the CN band between λ 4144 and λ 4184, plus greater NaD line strengths and λ 4227 strength than the sun. Whipple (1935) makes the first quantitative synthesis of color indices, line profiles and "line intensities" (half equivalent widths) for λ 3933, λ 4101, λ 4227, and λ 4340. He assumes the same giant/dwarf ratio as in the solar neighborhood but increases the percentage of light from G and K stars to agree with color and λ 3933 observations; he concludes that the line profiles calculated are broader and "hazier" than in simple giant spectra, leading early spectroscopists to classify spectra as "dwarflike". However, Whipple notes that his model does not predict the observed enhanced strengths of lines of neutral elements (NaI and CaI), nor does his prediction of strong CN bands agree with Öhman's (1934) observation.

More recently Morgan and Mayall (1957) in their qualitative visual classification of spectra of ellipticals and particularly

of the Sb spiral M31 state the principal contributors to the light are giants in the range G8 to M. The ratio of G8 to K3 dwarfs to giants of 40 to 1 in the solar neighborhood is acceptable, but the ratio is certainly no more than that and a smaller ratio would be more in accordance with spectral appearance. Spinrad (1962) constructs a synthesis of the M31 nucleus with G0 V, K0 III, and M1 V stars to match estimates of the strengths of features at 4226 Å and 5890 Å and to minimize residuals with Stebbins and Whitford's (1948) six color measures. The model selected has 10% of the visual light from G0 V stars, 50% from K0 III, and 40% from M1 V. The M dwarf contribution in this model is much greater than in our galaxy; Spinrad suggests either a normal age and an initial luminosity function heavily weighted to lower mass stars, or age so great that stars are now leaving the main sequence near K0 V. A subsequent search by Whitford (1964) for the NaI 8183-95 lines, which should be enhanced in some galaxies if M1 V contributes so strongly, reveals no traces; Whitford concludes that M dwarfs are not as prominent a contributor to the integrated light as claimed by Spinrad.

A disagreement also exists in interpretation of color indices. Roberts (1956) first discusses the difference in spectral energy distribution and M/L ratio between the elliptical M32 and

globular clusters; then he constructs synthetic color indices and M/L ratios by adding large numbers of K and M dwarfs to averaged measures of globular clusters. Agreement with Stebbins and Whitford's (1948) six color measures of M32 is within $0^{m}.05$; the constructed M/L is 85, in good agreement with values of 100-200 then available. As already mentioned, Baum (1959a, 1959b) synthesizes a different model to fit the same color observations; he finds it unnecessary to augment the lower main sequence for a good fit to colors. His best model of primarily old disk population stars has one third of the visual light from giants, with the remainder from subgiants and near main sequence stars.

Indications of an initial luminosity function unlike that in our galaxy also exist in M/L studies. Oort's (1940) investigations use early, rough observations of the light distribution, rotation curve, and velocity dispersion of the E7 elliptical NGC 3115 (now classified S0). Many models are investigated but all lead to a M/L ratio in the range 20-250, much higher than the value of 1-2 in the solar neighborhood. Oort suggests either a very large number of dwarfs with M/L of 200 or large amounts of interstellar gas or dust; Oort calculates that if gas and dust are in the relative proportions found in our galaxy, the optical depth would be only

a few parsecs, in conflict with observations. Schwarzschild (1954) combines the high tabulated M/L (100-300) with the red color indices to conclude that the bulk of the total luminosity in ellipticals is contributed by either K giants or K dwarfs, and the bulk of the mass either by faint dwarfs or by stars originally bright but now evolved and faint. He suggests three possible luminosity functions: (1) Light is mainly produced by K dwarfs and mass is from very faint dwarfs. The luminosity function is similar to the solar neighborhood, but shifted to fainter luminosities by five magnitudes. (2) Light is mainly produced by K giants and the mass is from faint dwarfs. The luminosity function must then rise very slowly from the K giants at zero absolute magnitude to the F stars at + 3, then rise very steeply at faint magnitudes in order that most of the mass be in stars of magnitude + 15 or fainter. (3) Light is produced by K giants and the mass is from evolved, exhausted faint stars with absolute magnitudes originally brighter than + 3. The initial luminosity function would be similar to the solar neighborhood but shifted seven magnitudes brighter, and peaked at magnitude +1 (implying a high frequency of stellar deaths early in the evolution of an elliptical).

Limber (1960) predicts upper limits to M/L for a simple, single age system by assuming that mass present initially forms stars instantaneously with a frequency in mass given by the initial luminosity function in our galaxy. He tabulates M/L as a function of time as stars leave the main sequence to become white dwarfs and interstellar matter, assuming light contributed during the giant phase is zero. The upper limit calculated at 12×10^9 years is M/L = 12; such a maximum is confortably high for the solar neighborhood and globular clusters, close for spirals, and too low by a factor of 3-10 for ellipticals. If giants contribute appreciable light, the discrepancy is greater. The observed M/L implies either that the ellipticals are 2-4 times as old as the age of the universe given by the Hubble constant, or that the model assumptions are in error. Limber prefers the alternatives that either the initial luminosity function in ellipticals must have many more dwarfs than in our galaxy or must have had many more massive stars which are now white dwarf stars.

All observational criteria appear to have certain disadvantages in practice. Photoelectric color indices are relatively easy and fast to measure, but difficult to correct for reddening by dust in our own galaxy and in the galaxy under observation. Among the more recent investigations, Tifft (1963)

minimizes reddening effects in our galaxy by choosing to observe at high galactic latitudes. He confirms earlier findings that the most luminous and massive ellipticals appear to be reddened toward their nuclei; it appears that both dust and population differences contribute to this effect, but it seems difficult to disentangle the two to obtain a quantitative evaluation of population differences. The Stebbins and Whitford (1948) six color observations of M32 are fitted directly with models by Roberts (1956), Baum (1959a, 1959b), and Spinrad (1962), none of whom discuss any reddening corrections despite the galactic latitude of 22^{o} and the probability that M32 appears to be seen through the disk of M31 and to be partly obscured (Holmberg 1953, Schwarzschild 1954).

M/L ratios are difficult to determine for ellipticals. They are determined by two separate fundamental observations; the mass is determined through difficult velocity dispersion measurements of spectra of the nuclei and the luminosity through large diaphragm measures of light from the entire elliptical. Mass and light measures do not necessarily refer to the same volume of space; the ratio is also dependent on knowledge of the distance, which is quite uncertain for galaxies too far to resolve directly and too near to have large red shifts. It is not surprising to find that M/L for M32 is quoted as 100-200 by Roberts (1956)

and 10.8 by Fish (1964) eight years later since uncertainties are large in the determinations.

In summary, there is general agreement that an elliptical is composed of an old stellar population; the possibility that the predominant population may be older than stars in our galaxy arises as one alternative in the spectrographic investigations of Spinrad and the M/L investigation by Limber. There is general agreement that most of the integrated light arises from a metal-rich stellar population, although a small percentage of the light may come from a metal-poor population. The initial luminosity function appears to be weighted either toward stars of less than solar mass or much more than solar mass (which are now white dwarfs); considerable disagreement exists on which is observationally the better alternative.

THEORETICAL CONSIDERATIONS

This section is devoted to discussion of models of elliptical galaxies. A model is defined here to be a set of mathematical and physical assumptions which simulate the stellar content of an elliptical galaxy; the purpose of making a model is to test understanding of elliptical galaxies by making predictions of observable quantities, equivalent widths of spectral features and M/L ratios. The parameters of particular interest are the initial luminosity function and age of ellipticals. After an opening discussion of modeling techniques, a power law form is introduced and assumed for the initial mass function and the initial luminosity function. The power law exponent is allowed to be continuously variable; each choice of exponent yields a different number versus mass relation created in the galaxy model. A discussion of the effect of age on stars formed in accordance with an assumed initial luminosity function results in models in which the numbers in each small section of a color magnitude diagram are calculated as a function of age and initial luminosity function, though this study is limited to the two ages represented

by the old galactic clusters NGC 188 and M67. Finally, equations are presented for deriving equivalent widths and M/L ratios for each model, i.e., each choice of age and power law exponent, n.

Interpretation of observations of integrated light differs in several important respects from observations of single stars. With single star observations, color magnitude diagrams may be made directly with no a priori assumptions about the stars involved. Magnitude and color measurements of any star are independent of other stars measured. In studying integrated light only the net effect of many stars is observed, hence models are required to compare the information received with a normal color-magnitude diagram. All such models inevitably carry with them the possibility of non-uniqueness; more than one model may fit the same set of measurable parameters. It is valuable to explore a range of models to find how wide a set of initial assumptions will yield acceptably small observational residuals; it is also important that the observational tests be of as many types as possible.

The simplest models are those in which a certain definite number of spectral and luminosity classes are chosen from prototypes in our galaxy. The relative number of stars in each class is the variable to be determined by comparison with

observations. In principle, the number of classes may exceed the number of observations; the preferred method for solution is linear programming (Gass 1964), with minimum residuals as optimization condition. In practice, experimental error is generally sufficient to make any solution mathematically impossible using the observed parameters as rigorous conditions in the equations. Linear programming techniques for finding solutions with variable conditions (experimental errors) in the equations are still in early stages of development (Cross, private communication); as numerical techniques improve, linear programming may develop into the preferred modeling technique for investigations of integrated light. When the number of spectral and luminosity classes is reduced sufficiently to equal or be less than the number of observations, a direct or least squares solution is possible for the number or relative number of stars in each class. Such direct or classical least squares solutions often yield meaningless solutions in the presence of experimental error, e.g., large negative numbers for some classes. Hence trial and error techniques, selective alterations to obtain better residuals, are used almost universally. A poor choice of starting spectral and luminosity classes or poor method of alteration can lead to a model with significantly larger residuals than necessary. More deterministic models are desirable, particularly

if such models are specifically tailored to answer the problems discussed in the introductory chapter.

The construction of models begins with the assumption that the nucleus of an elliptical galaxy can be compared meaningfully with clusters formed in a single generation in our galaxy. It is recognized that the nucleus is in a unique dynamic position; even if it originated as a single generation of stars, highly elliptical orbits of stars formed at larger radii would add stellar interlopers. Primeval gas remnants and gas ejected from evolving stars could concentrate near the nucleus, possibly forming later generations of stars. Nevertheless, considerable progress in understanding galaxy nuclei might be made by starting with the simplest assumptions, constructing models to check against observations, then deriving more elaborate models.

The papers by Morgan and Mayall (1957), Tifft (1963), Baum (1959a, 1959b), and van den Bergh and Henry (1962) suggest that models based on old, metal-rich stars may represent most of the light from elliptical galaxies. Metal-poor stars may be present and contribute a small fraction of the light; they are probably not the principle contributors, but may be the first corrections to consider to a simple model. Obvious requirements for single generation models are a variable age and a variable

initial luminosity function. As a group of stars ages, the integrated light changes in character and quantity. Papers by Schwarzschild (1954), Limber (1960), Roberts (1956), and Spinrad (1962) suggest that the initial luminosity function should not be limited to that in our galaxy.

The initial mass spectrum may be a function of the temperature, density, turbulence, composition, and magnetic field strength in the gas from which stars form. Ideally a fully developed theory would give the initial mass spectrum as a function of these parameters; it would then be possible in principle to vary the initial physical variables, predict an initial mass spectrum, correct for age and other physical processes, compare predicted observational parameters with real observations, and thus obtain the range of initial physical variables consistent with observations. A simplified derivation of the initial mass spectrum exists (Kruszewski 1961) based on Jeans' instability criterion; the equation derived involves a single adjustable parameter, the minimum mass star formed, which in turn depends on the density of material and velocity of sound in the original medium. Although arbitrary selection of a minimum mass of 0.07 solar masses by Kruszewski yields excellent agreement with observation of our galaxy, the simple theory used actually predicts considerably

larger masses (10^3 - 10^{11} solar masses) and does not satisfy Poisson's equation (Arny 1965). No complete theory appears to be published as yet which is free of these defects. Therefore, in this study a simple power law form is chosen for the initial mass function, which also can be made to fit observations of our galaxy over the range 0.4 to 10 solar masses.

The initial mass function $\xi(m)$ (Salpeter 1955) in our galaxy obeys the relation

$$\xi(m) = C_1 \left(\frac{m}{m_\odot}\right)^n$$

where $\xi(m)$ is the number of stars per cubic parsec per log mass interval, c_1 a density factor (0.03 in the solar neighborhood), $\left(\frac{m}{m_\odot}\right)$ the mass in solar units and n an empirical constant (-1.35 in our galaxy, between 0.4 and 10 solar masses). This is related to the more convenient initial luminosity function by the expression:

$$\psi(M_V) = C_2 \left(\frac{m}{m_\odot}\right)^n \frac{d \log m}{d M_V}$$

where ψ (M_V) is the number of stars per cubic parsec per magnitude interval (M_V $-1/2$, M_V $+ 1/2$), and c_2 a density factor. The dependence on mass is to be varied in the models through varying n.

To give some insight into the variation involved, the following table lists the ratio ψ (M_V) at the tabulated n divided by ψ (M_V) at n = -1.35, the initial luminosity function exponent for our galaxy, evaluated at M0 V (M_V=+ 9):

TABLE 1

RATIO at M0 V of ψ (M_V) at n/ψ (M_V) at n = -1.35

n	Ratio	n	Ratio
-6	25	-1.35	1.00
-5	13	-1	0.79
-4	6	0	0.39
-3	3	1	0.20
-2	1.6	2	0.10

Table 2 lists ψ (M_V) as a function of M_V and n.

TABLE 2

Ψ (M_V) AS A FUNCTION OF n

M_V \ n	2	1	0	-1	-1.35
- 6	33,300.	360.	3.89	.0420	.0085
- 5	8,730.	174.	3.48	.0693	.0176
- 4	2,180.	82.1	3.09	.116	.0368
- 3	629.	41.5	2.74	.181	.0700
- 2	209.	22.6	2.44	.264	.121
- 1	79.7	13.2	2.20	.364	.194
0	31.5	7.91	1.99	.499	.308
1	13.9	4.95	1.76	.623	.434
2	7.24	3.36	1.56	.723	.555
3	3.60	2.21	1.35	.831	.699
4	1.84	1.46	1.16	.920	.849
5	1.	1.	1.	1.	1.
6	.659	.776	.915	1.08	1.14
7	.449	.623	.866	1.20	1.35
8	.342	.563	.927	1.53	1.82
9	.257	.513	1.02	2.04	2.60
10	.178	.447	1.12	2.82	3.89
11	.124	.393	1.24	3.93	5.89
12	.0846	.337	1.34	5.34	8.66
13	.0532	.274	1.42	7.30	13.0
14	.0315	.216	1.49	10.2	20.1
15	.0189	.170	1.54	13.9	30.1

TABLE 2---Concluded

M_V \ n	-2	-3	-4	-5	-6
- 6	.0005	0	0	0	0
- 5	.0014	0	0	0	0
- 4	.0044	.0002	0	0	0
- 3	.0120	.0008	0	0	0
- 2	.0285	.0031	.0003	0	0
- 1	.0604	.0100	.0017	.0003	0
0	.127	.0315	.0079	.0020	.0005
1	.221	.0784	.0278	.0099	.0035
2	.337	.156	.0727	.0337	.0157
3	.509	.312	.191	.117	.0719
4	.731	.581	.461	.366	.291
5	1.	1.	1.	1.	1.
6	1.27	1.50	1.76	2.08	2.45
7	1.68	2.32	3.23	4.48	6.23
8	2.51	4.14	6.81	11.2	18.5
9	4.08	8.14	16.2	32.4	64.6
10	7.08	17.8	44.7	112.	282.
11	12.4	39.3	124.	394.	1,250.
12	21.3	84.6	337.	1,340.	5,340.
13	37.6	194.	1,000.	5,160.	26,600.
14	70.4	484.	3,330.	22,900.	157,000.
15	125.	1,130.	10,200.	92,000.	830,000.

The initial luminosity function is not observed directly in galaxies because it is modified by stellar evolution. The current M_V and B-V of each portion of the initial mass function must be known in a color magnitude diagram in order to calculate equivalent widths and mass to light ratios. Very massive stars are now white dwarfs; their original mass is added to the total mass to calculate M/L but light output is neglected. A few less massive stars are now on the giant branch; their relative number per magnitude and B-V interval must be calculated carefully because they contribute a substantial fraction of the total light. Still less massive stars are close to the main sequence, and the least massive stars are very close to the initial main sequence.

The problem to be solved is to connect each small section (M_V) of the initial luminosity function to its current (M_V, B-V) position in the color magnitude diagram. If a suitably spaced sequence of perfect stellar evolution tracks existed, it would be necessary only to take the loci of constant time in the ($\log L_{bol}$, $\log T_e$) plane, transform to the (M_V, B-V) plane, then take the numbers of stars from ψ (M_V) above in order to predict observable properties at any given age and initial luminosity function. Unfortunately, such complete tracks do not exist for the mass range 0.1 to 1.2 $M_\odot$ for which models are desired.

There are no modern models going to the high luminosity end of the giant branch. The tracks for the subgiant branch (Demarque and Larson 1964, Hallgren and Demarque 1966, and Iben 1967) yield color magnitude diagrams differing significantly from observations; near the main sequence, agreement with observations is much better. It is necessary to blend theoretical tracks with observations of clusters and the initial main sequence to obtain the best models possible at present.

The construction of models follows Sandage's (1957b) method for semi-empirical determination of evolutionary tracks in principle. Large scale (M_V, B-V) plots are made of the observed stars in two old galactic clusters NGC 188 (Sandage 1962a) and M67 (Johnson and Sandage 1955, Eggen and Sandage 1964). A single curve is drawn through the observed points; for NGC 188 it is a curve through normal points in Table 4 of Sandage (1962a). Since no normal points are tabulated with the new photoelectric measures of M67 (Eggen and Sandage 1964), the older normal points (Johnson and Sandage 1955) are corrected to the new distance modulus, plotted, shifted slightly where necessary to obtain a better fit to the more recent data, and a continuous curve drawn. These cluster curves must be related to the original M_V's on the main sequence. The individual evolutionary tracks for stars of mass 0.95, 1.0,

1.03, and 1.20 $M_\odot$ taken from Demarque and Larson (1964) and Hallgren and Demarque (1966) are transformed to (M_V, B-V) plots by applying bolometric corrections and the (log Te, B-V) relation in Sandage's Table A2 (1962b). A small correction is also applied to B-V to shift the tracks from the theoretical zero age main sequence to the observed zero age main sequence in Sandage's Table 3 (1962b). The shapes of these evolutionary tracks resemble each other closely over the ranges of hundredths of a solar mass between them; hence interpolation between these tabulated tracks should result in acceptably small errors.

Such interpolated tracks are constructed at intervals of $0.^m1$ from just below the turnoff point in NGC 188 and below the "gap" in M67 down as faint in magnitude as the cluster photometry permits. It is assumed that the clusters merge smoothly with the zero age main sequence at absolute magnitude +.7, three to four magnitudes below the turnoff points. The region of the turnoff point, the subgiant and giant branches cannot be accurately treated with existing theoretical models. Therefore it is assumed that both clusters arise from the initial luminosity function found in our galaxy by combining data for star clusters (van den Bergh 1957, Sandage 1957a), evolutionary effects on stars in the solar vicinity (Sandage 1957a), and fainter unevolved stars in the solar vicinity. The tabulation of

the initial luminosity function used is that in Limber's Table 3 (1960). The initial luminosity function is scaled to the cluster population by requiring that the sum of the stars in the initial luminosity function in a one magnitude interval below the turnoff point be the same as the sum of the stars in the same magnitude interval in the cluster, after correcting the cluster for evolution away from the main sequence. Direct counts are made in NGC 188 for this purpose, and the observed luminosity function in Table 8 (Sandage 1957a), corrected to the new distance modulus (Eggen and Sandage 1964), is used in M67.

After this normalization the number of stars evolving from any magnitude interval on the initial main sequence is known; it is necessary only to count the number of stars along the cluster subgiant and giant branches and find the corresponding sum along the normalized initial luminosity function to know the original M_V. In practice, $0.^m04$ is a convenient interval in both clusters. The expected sums of numbers of stars are tabulated from the initial luminosity function beginning at the last computed track; the corresponding sums are counted along each cluster curve and marked as the end point of evolution from that magnitude on the main sequence. In this way a table for each cluster (Tables 3 and 4) is built of a magnitude on the initial main sequence with its associated cluster magnitude and B-V.

TABLE 3

NGC 188 AND MAIN SEQUENCE CORRESPONDENCE

$M_{V\,M.S.}$	$M_{V\,188}$	$(B-V)_{188}$	$M_{V\,M.S.}$	$M_{V\,188}$	$(B-V)_{188}$
7.00	7.00	1.04	5.06	3.99	0.62
6.90	6.83	1.01	5.02	3.93	0.63
6.80	6.62	0.98	4.98	3.90	0.63
6.70	6.50	0.94	4.94	3.88	0.64
6.60	6.33	0.91	4.90	3.86	0.65
6.50	6.17	0.88	4.86	3.85	0.66
6.40	6.00	0.85	4.82	3.85	0.68
6.30	5.83	0.81	4.78	3.85	0.71
6.20	5.67	0.78	4.74	3.89	0.79
6.10	5.50	0.75	4.70	3.90	0.84
6.00	5.30	0.73	4.66	3.96	0.92
5.90	5.14	0.71	4.62	3.92	0.96
5.80	4.97	0.69	4.58	3.70	1.01
5.70	4.80	0.67	4.54	3.40	1.03
5.60	4.65	0.65	4.50	3.00	1.06
5.50	4.52	0.63	4.46	2.56	1.10
5.40	4.41	0.62	4.42	1.87	1.16
5.30	4.32	0.62	4.38	1.36	1.23
5.20	4.17	0.62	4.34	1.03	1.29
5.10	4.04	0.62			
			4.30	0.0	1.6

TABLE 4

M67 AND MAIN SEQUENCE CORRESPONDENCE

M_{V} M.S.	M_{V} M67	(B-V) M67	M_{V} M.S.	M_{V} M67	(B-V) M67
7.00	7.00	1.04	5.50	5.24	0.68
6.90	6.88	1.01	5.40	5.13	0.61
6.80	6.77	0.99	5.30	5.01	0.64
6.70	6.65	0.97	5.20	4.89	0.63
6.60	6.53	0.94	5.10	4.78	0.61
6.50	6.41	0.91	5.00	4.66	0.60
6.40	6.30	0.89	4.90	4.57	0.58
6.30	6.18	0.86	4.80	4.47	0.57
6.20	6.06	0.84	4.70	4.37	0.56
6.10	5.95	0.81	4.60	4.26	0.55
6.00	5.83	0.79	4.50	4.15	0.54
5.90	5.71	0.77	4.40	4.06	0.53
5.80	5.60	0.74	4.30	3.97	0.53
5.70	5.48	0.72	4.20	3.90	0.52
5.60	5.36	0.70	4.10	3.78	0.52

TABLE 4—Concluded

$M_{V_{M.S.}}$	$M_{V_{M67}}$	$(B-V)_{M67}$	$M_{V_{M.S.}}$	$M_{V_{M67}}$	$(B-V)_{M67}$
4.06	3.75	0.52	3.46	3.05	0.55
4.02	3.72	0.51	3.42	3.03	0.57
3.98	3.69	0.51	3.38	3.03	0.60
3.94	3.64	0.51	3.34	3.06	0.65
3.90	3.60	0.51	3.30	3.17	0.71
3.86	3.56	0.51	3.26	3.28	0.75
3.82	3.52	0.51	3.22	3.42	0.80
3.78	3.29	0.51	3.18	3.50	0.86
3.74	3.27	0.51	3.14	3.43	0.90
3.70	3.25	0.51	3.10	3.25	0.92
3.66	3.23	0.51	3.06	2.55	0.96
3.62	3.20	0.52	3.02	2.13	0.98
3.58	3.16	0.52	2.98	1.67	1.02
3.54	3.12	0.53	2.94	1.13	1.07
3.50	3.08	0.54	2.90	0.68	1.16
			2.86	0.15	1.32
			2.82	-0.5	1.6

Neither NGC 188 or M67 is a rich cluster, both have thinly populated giant branches. Examination of a field star color magnitude diagram (Wilson 1959) suggests that the giant branch of more populated clusters might well extend into the early M stars. Alternate models, labelled NGC 188+M and M67+M, are used throughout all investigations. Each is identical with the normal cluster model except that one additional evolutionary track into the M stars is added; the addition of this track probably overestimates the number of M giants present in richer clusters, but is useful as a limiting case. Since NGC 188 is at the lower envelope of field stars in a color magnitude diagram, the additional track is added near the extreme lower limit at $M_V = 0.0$, $B-V = 1.6$. The M67 giant branch appears to parallel the NGC 188 branch about $0.^m5$ brighter, so the M67+M model is assumed to have an additional track terminating at $M_V = -0.5$, $B-V = 1.6$. By use of these indirect methods the positions at two ages on the evolutionary paths of stars of small mass are determined.

The models which allow variability in initial luminosity function and age are complete; they may now be used to predict equivalent widths and M/L ratios. The general form of the equation for integrated equivalent widths (de Vaucouleurs 1958) is:

$$\overline{EW} = \frac{\sum_i N_i L_\lambda \; EW_i^* \; 10^{-0.4 M_{V_i}}}{\sum_i N_i L_\lambda \; 10^{-0.4 M_{V_i}}}$$

where $\overline{EW}$ is the model's equivalent width, Ni the number of stars of luminosity and spectral class i (given by $\psi(M_V)$ as modified by stellar evolution), L_λ a correction factor for the relative level of the continuum at wavelength λ (normalized at 5450 Å (Willstrop 1965), and EW_i^* the measured equivalent width of the spectral feature at wavelength λ of a star in class i.

The models are extended over the range 0.1 to 100 solar masses to calculate the mass to light (M/L) ratio. The M/L ratio is particularly useful in revealing the presence of objects which are relatively non-luminous, but sufficiently numerous to add appreciably to the total mass. The equation for synthesizing the visual mass to light ratio in solar units is:

$$\frac{M}{L} = \frac{\sum_i N_i \left(\frac{m_i}{m_\odot}\right) + \sum_j N_j \left(\frac{m_j}{m_\odot}\right)}{\sum_i N_i \; 10^{-0.4 (M_{V_i} - M_{V_\odot})}}$$

in which $\left(\frac{m_i}{m_\odot}\right)$ is the mass of a star in class i in solar units, and $M_{V_\odot}$ is the absolute magnitude of the sun (Allen 1963). Stars originally at the upper end of the main sequence are assumed to be non-luminous interstellar matter and white dwarfs. All mass is assumed to be retained and added to the total mass, hence N_j is the number of stars on the initial luminosity function in class j beyond the giant branch in evolution of the model and $\left(\frac{m_j}{m_\odot}\right)$ the mass of a star in class j.

Substitution of a constant times Ni and Nj in either equation does not affect the final calculated value, hence the absolute number of stars of each class cannot be determined through observations of $\overline{EW}$ or M/L. Only relative numbers of stars in each class can be determined in principle by observing equivalent widths; this fact also allows N to be normalized at will for convenience.

The only quantities still to be determined are the equivalent widths of spectral features of stars (EW_i^*) and of galaxies.

OBSERVATIONS

The equation for synthesis of equivalent widths developed in the last section requires measurements of equivalent widths at the M_V and B-V of stars in the clusters NGC 188 and M67. Ideally, spectra would be taken of stellar members of the clusters, but the individual stars are so faint that excessive prime observing time would be required. MK standard stars are observed instead of cluster members; spectroscopic investigations by Greenstein and Keenan (1964) and Sandage (1962a) indicate no important differences between members of the clusters and MK standards.

The choice of elliptical galaxies to be observed would appear to be arbitrary, but in reality is quite limited. The spectrograph and plate combination available is fairly slow, hence only a few of the brightest galaxies can be observed with single night exposures. A few of the brightest galaxies have individual mass determinations; the four selected for investigation are NGC 221 (M32) a dwarf elliptical, NGC 3115 classified E7 for many years but now classified S0, NGC 3379 an intermediate mass E1, and the giant NGC 4472. Properties of importance to this investigation are listed in Table 5.

TABLE 5
GALAXY PROPERTIES

NGC	TYPE	Vr (km/sec)	B(0)	MASS ($M_\odot$)	$(M/L)_V$	D(0) (min. arc)
221	E2	-213	9.39	2.95×10^9	10.8	3.2
3115	$E7/S0_1$	646	10.43	8.7×10^{10}	27.	2.8
3379	E1	877	10.83	9.6×10^{10}	10.8	2.3
4472	E1	948	9.84	1.1×10^{12}	19.2	4.5

Type, radial velocities Vr, integrated blue magnitudes B (0), and diameters D(0) are from de Vaucouleurs and de Vaucouleurs Catalog (1964); masses and M/L are from Fish (1964) except for NGC 3115, where mass is from Pskovskii (1965) and M/L from Limber (1960). Exposure lengths are 2 to 6 hours on IIa-O (unbaked) plates. From inspection of published luminosity profiles (e.g., Figure 2 in Fish, 1964) it appears that the principal contribution to the exposure must be from the innermost 10" to 20" of the diameter of the elliptical, with little contribution from outside this nucleus.

All observations are made with a single system, the Newtonian spectrograph of the 36" Steward Observatory reflector located on Kitt Peak. The spectrograph is described by Carpenter (1963). The dispersive element used is an echelle transmission grating mounted on the face of a crown glass prism, followed by an f/0.8 Schmidt camera; the net effect is a nearly constant

dispersion of approximately 265Å/mm from 4000Å to 6600Å. All "blue" spectra from 4000Å to 4600Å are made on IIa-O (unbaked) plates developed 3-1/2 minutes in D-19. All spectra are widened by trailing.

Intensity calibration on all plates is accomplished by trailing the star or galaxy across calibrated Kodak neutral density filters placed along the slit. Plate tracing is on the Hilger and Watts Recording Microphotometer at the Steward Observatory. A number of tracings are then superimposed on a light table, and a pseudo-continuum drawn on each tracing in accordance with a simplified form of the method used by Schwarzschild, Schwarzschild, Searle, and Meltzer (1957). Details of the intensity calibrations and reduction procedures are in Appendix I.

The choice of the spectral features to be used is a difficult one. Both the MKK Atlas (1943) and the Meinel Schulte Atlas (1967) are used as guides for features to investigate in the blue, and Fehrenbach's (1958) review article for features to investigate in the yellow and red. At 265Å/mm blending is a severe problem; every potentially useful feature is a blend, usually a very complex one. The greatest care is used to be certain that the same range of wavelength is always measured over the full range of spectral and luminosity types used. Master

tracings are marked with the most reproducible features, then individual tracings carefully marked from the master. If a prominent feature is partially blended with the guide feature, the spectral interval is usually chosen to include both in order to minimize effects of focus variations and of blending due to velocity dispersion of the stars in galaxy nuclei. The nomenclature for this interval is the rough wavelength of the guide line, but the interval measured will not be centered on this guide wavelength. As an example, the Sr II 4077 feature certainly includes (and is often dominated by) Fe I 4071. Most features undoubtedly include weak iron or titanium lines (Westerlund, private communication). A table of precise wavelengths and wavelength intervals would be required to reproduce these measurements with another spectrograph; however, any change in resolution would alter so many features that such a table would not be useful. Because of the severe blending, the equivalent width measurements should not be used in any other type of investigation.

The observations include 526 equivalent width measurements from 42 stellar plates and 169 measurements from 13 galaxy plates. Appendix I contains the detailed results

for stars in Table 6 and for galaxies in Table 7; the equivalent widths for stars are plotted in Figures 9 through 16. The ordinate is B-V, not corrected for reddening, and the abscissa is equivalent width in Å. For example, λ 4226 is plotted in Figure 1. B-V is plotted in preference to spectral type because B-V is more closely related to the cluster color magnitude diagrams constructed and because B-V is a more accurately determined parameter than spectral type. Luminosity Class III, IV, and V stars are bright, nearby stars not appreciably reddened (Johnson 1966), however, Class I and II stars have probably been shifted horizontally to the right by reddening (equivalent widths are unaffected). Corrections for reddening are not important for the cluster models because only Classes III, IV and V are used. Each point of the graphs is a single measurement of a single plate of one star, with three exceptions which are the average of two observations. For these stars the separate results agreed to $\pm$ 10%.

All features have some dependence on both temperature and luminosity. The most useful features for temperature determination are those with the largest slopes and for luminosity determination the largest separation between Classes V and III. Particularly noteworthy are 4175, 4200, 4226, 4254, 4275, and

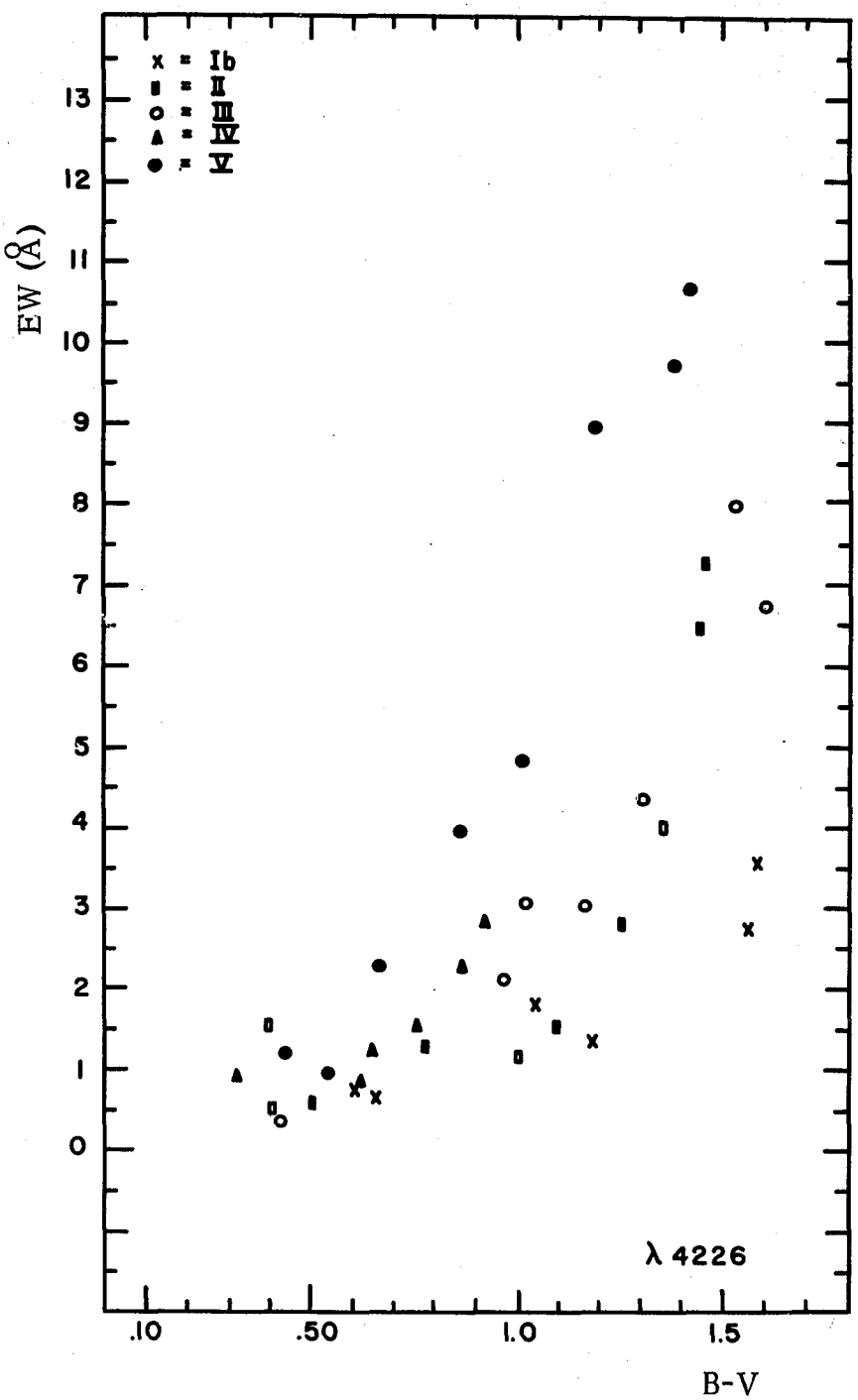

Fig. 1--Equivalent Widths (Å) vs. B-V for λ 4226.

4300. In typical blends in late type stars a neutral element is a strong contributor, hence most features become stronger with decreasing stellar surface temperature. The hydrogen lines are important exceptions to this trend, since they decrease with decreasing temperatures. The G band (4300) is also interesting in that it is double valued; the color of the turnover point depends on luminosity, and is at the highest temperature for the lowest luminosity.

The spectra of galaxies are reduced in a very similar fashion. Since they can not be widened as much as stellar plates three plates are taken. Each plate is traced and reduced quite independently of the other plates of the same galaxy, then the results for each blend averaged. The standard deviation is tabulated for each feature, then the root mean square of the internal standard deviation is calculated for each galaxy from the standard deviations of all features.

CONCLUSIONS

This section gives the determination of the range of age and initial luminosity functions in elliptical galaxies consistent with observations of mass to light ratios and equivalent widths of spectral features. Parameters available for adjustment are two values of age and continuous variation of n, the initial mass function exponent. The quality of fit is judged by analysis of average deviation (AD) and root mean square error (RMSE).

The definitions of AD and RMSE used are:

$$AD = \frac{\sum_{i=1}^{N} (\overline{EW}_i^{\circ} - \overline{EW}_i)}{N}$$

$$RMSE = \sqrt{\frac{\sum_{i=1}^{N} \sum_{j=1}^{m} (EW_{ij}^{\circ} - \overline{EW}_i)^2}{Nm}}$$

in which EW_{ij}° is the j^{th} measurement of the i^{th} equivalent width, $\overline{EW}_i^{\circ}$ is the mean observed value of each spectral feature, $\overline{EW}_i$ is the predicted width for a given age and power law exponent, the sum in i is over the total number (N) of spectral features used, and the sum in j is over the number (m) of individual measures of

each feature used. The calculations are performed for each set of measures of each galaxy and each choice of age and initial luminosity function.

Figures 2 through 5 present AD and RMSE results for NGC 221, 3115, 3379, and 4472, the four galaxies investigated in this dissertation. The complete tabular data are in Appendix 2. The ordinate is equivalent width in Ångstroms, the abscissae is n (the power law exponent of the initial mass function), plots representing each model (M67, M67 + M, NGC 188, NGC 188 + M) are given for each galaxy. The more negative values of n represent dwarf enriched models.

A perfect fit of a model, with all parameters continuously variable, to errorless observations would yield AD and RMSE simultaneously zero at the same age and n and nowhere else. When limited models are used and experimental errors enter, only an approximation to these criteria can be expected, minimum RMSE and AD approximately zero. An AD near zero is not a sufficient condition for a good fit, since positive and negative residuals in combination may yield an AD near zero for a spurious fit. The RMSE avoids this objection; it is intrinsically positive and is minimum for the best fit of model to observations. Most of the features measured in stellar spectra and used here increase

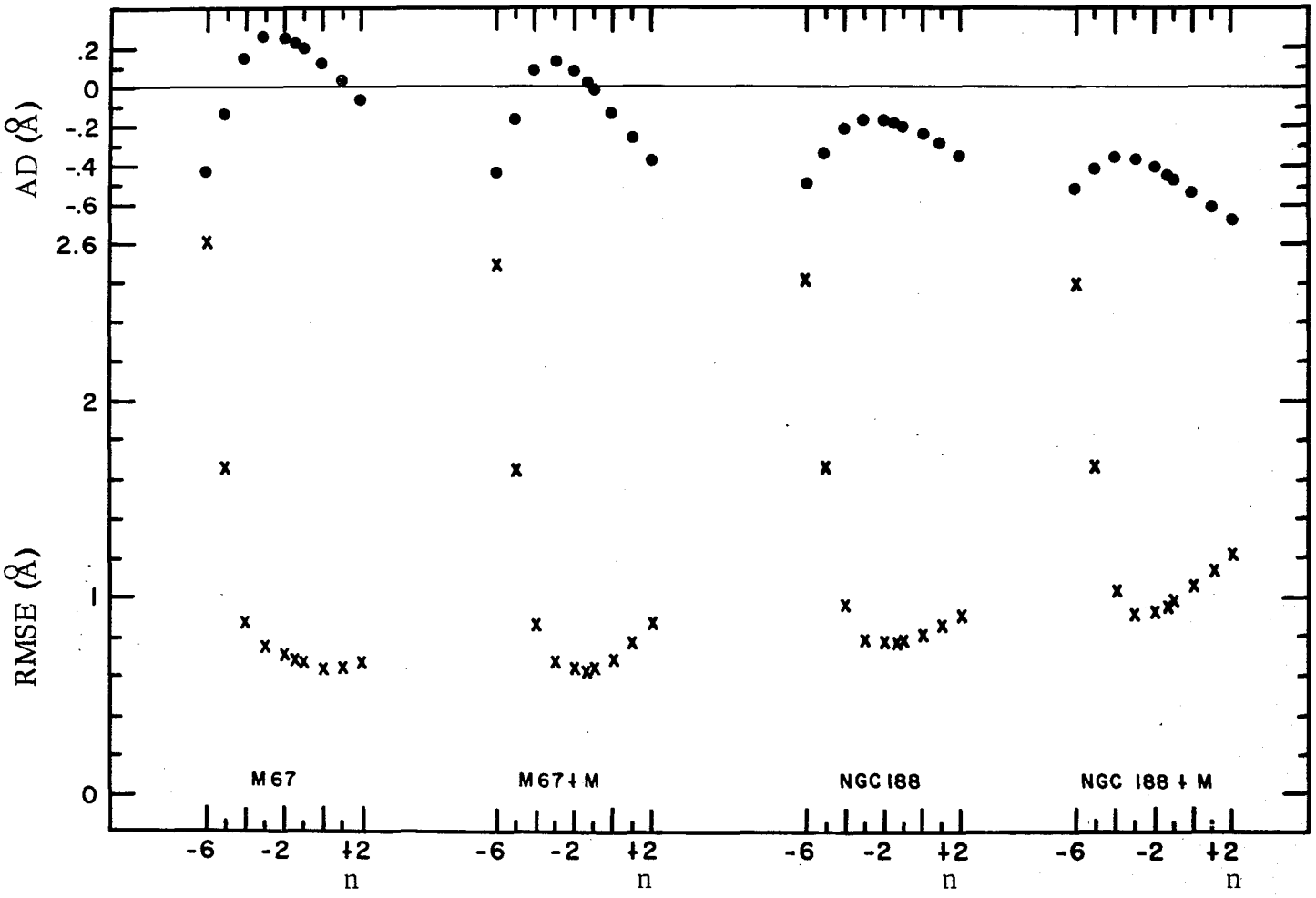

Fig. 2--NGC 221, AD and RMSE vs. n.

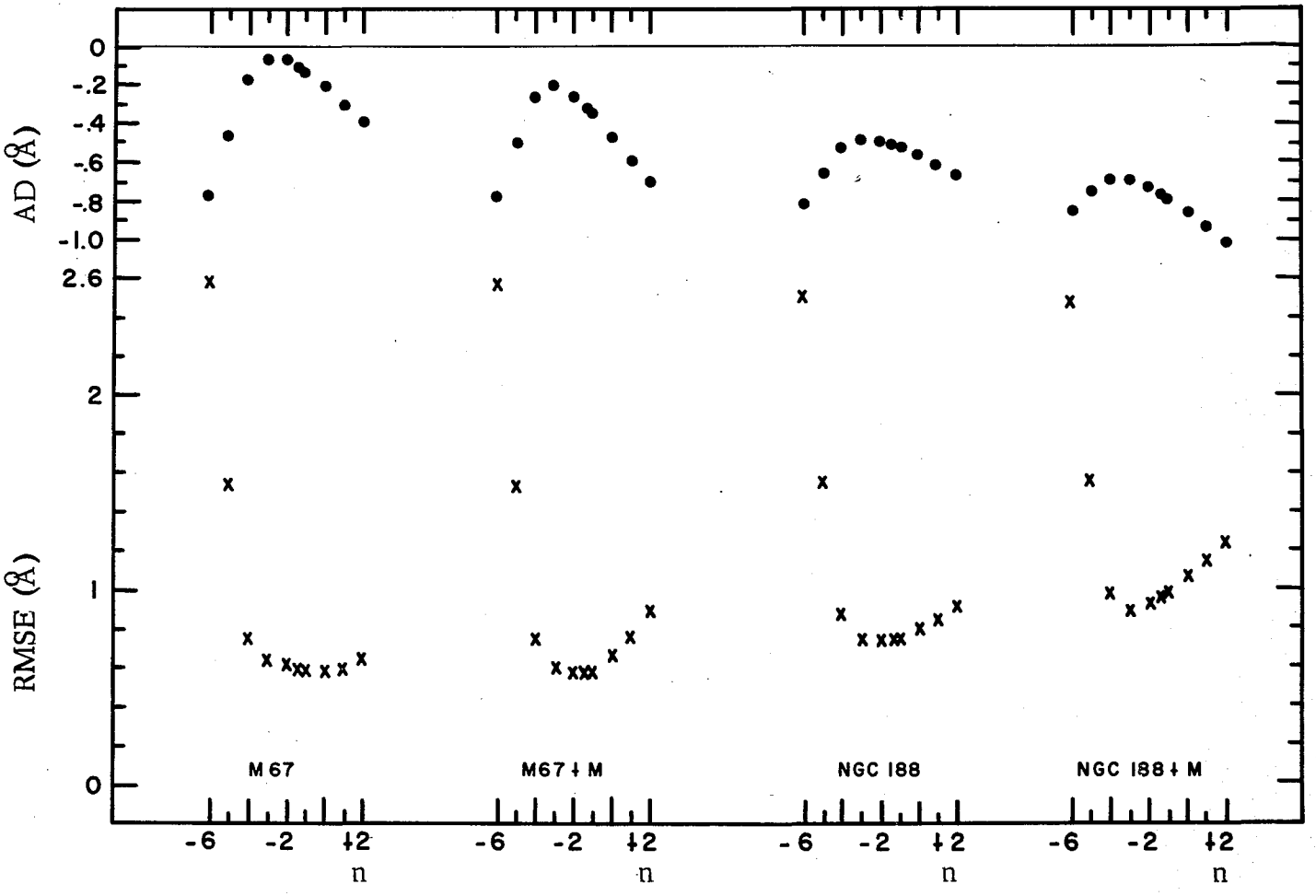

Fig. 3--NGC 3115, AD and RMSE vs. n.

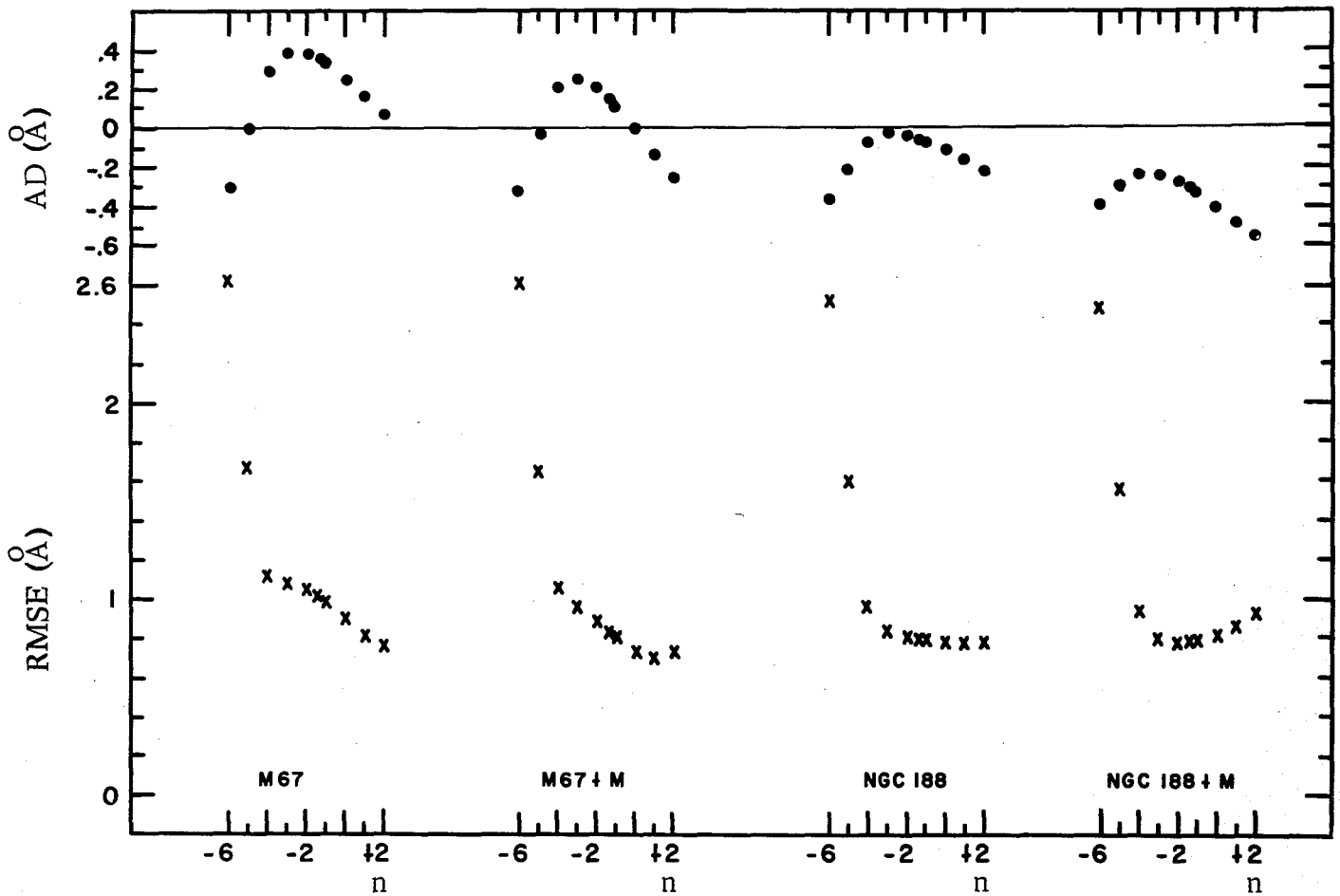

Fig. 4--NGC 3379, AD and RMSE vs. n.

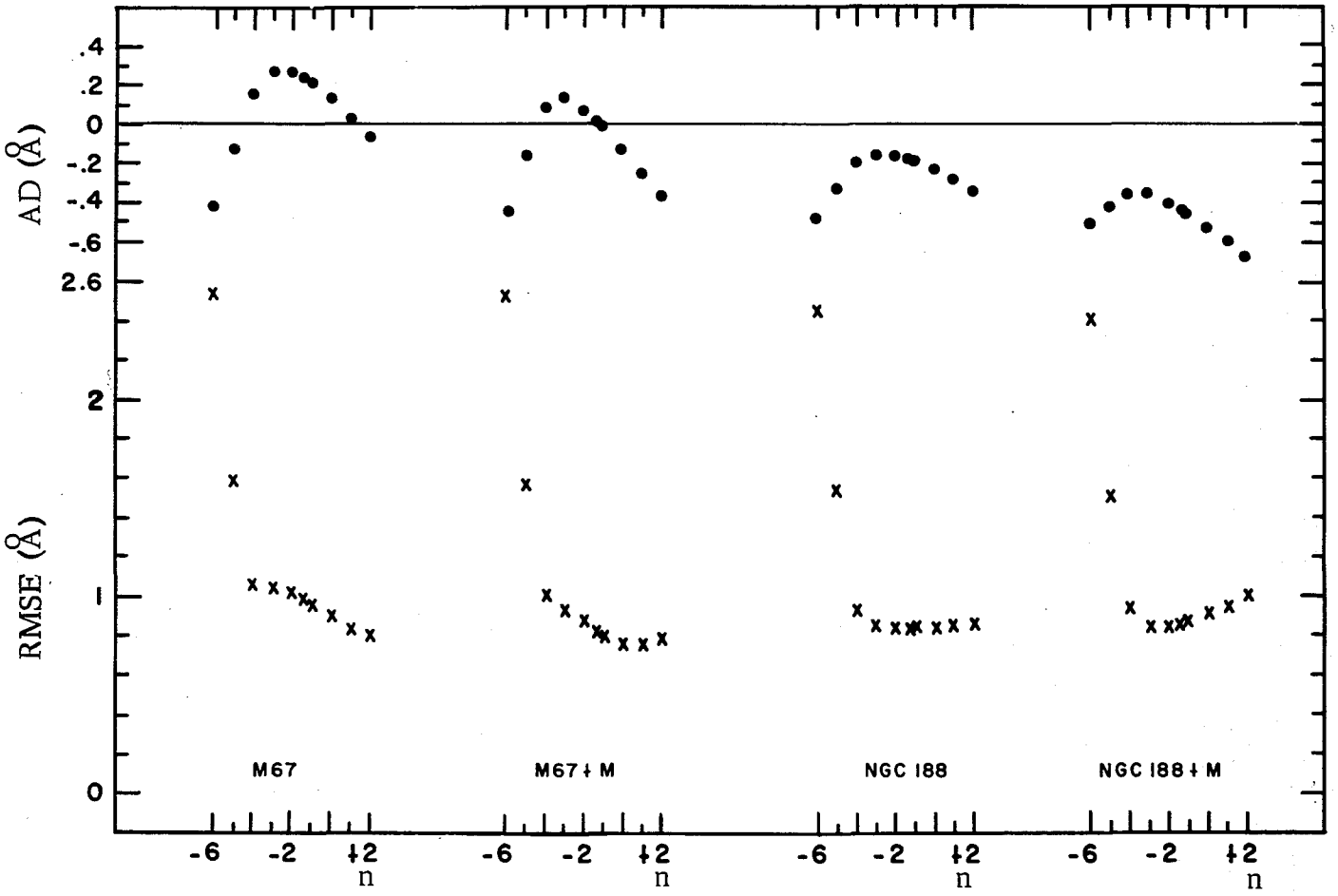

Fig. 5--NGC 4472, AD and RMSE vs. n.

with increasing B-V, hence increase also with increasing age (since one effect of increasing age is that the more luminous parts of the color magnitude diagram appear to shift to greater B-V). These features dominate when averages are calculated, and the AD curve tends to be shifted more negative (downward) with increasing age. Adding an M star track to obtain an upper limit to M star contributions also results in increased equivalent widths and more negative AD, although the effect is smaller than the effect due to age.

Figure 2 is a plot of AD and RMSE vs. n for NGC 221. The minimum RMSE occurs at n = -1.35 in the M67 + M type of model, with zero AD between n = -1 and -1.35; the best luminosity function fit for NGC 221 is close to the value -1.35 deduced for our galaxy. In all four models RMSE increases rapidly for n less than -3, hence enrichment of M0 V dwarfs by more than a factor of 3 (Table 1) appears unlikely in NGC 221. In Figure 3 for NGC 3115 the minimum RMSE occurs at n = -1.35 and n = -2 in the M67 + M type of model, with significantly increased RMSE for n less than -3. However, AD is not zero in any of the four types of models. Figure 4 for NGC 3379 is similar to Figure 5 for NGC 4472. In both figures the minimum RMSE occurs at n=+1 in the M67 + M type of model, this n

corresponds to dwarf depletion by a factor of 5 at M0 V. RMSE for the -1.35 exponent model is 0.10Å (14%) larger for NGC 3379 and 0.08Å (11%) larger for NGC 4472 than for the $n = +1$ exponent model; these differences are of marginal significance. In both figures RMSE increases rapidly for dwarf enriched models.

It is evident that for all four galaxies the best initial luminosity function (for minimum RMSE) is quite close to that in our galaxy, $n = -1.35$. A lower main sequence enriched with dwarf stars is apparently ruled out with the assumptions of a single age and a power law mass function. Actually the best fit for the intermediate mass elliptical NGC 3379 and giant NGC 4472 is a somewhat dwarf depleted model, although the differences in residuals are marginal. Equivalent widths are much less affected by dwarf depletion than by dwarf enrichment. A form of mass dependent evaporation (King 1963) which is relevant for dwarf depletion may apply to galaxy nuclei. Ideally this effect on the initial main sequence should be considered to see if a better fit to observations would result.

In addition to the statistical indicators AD and RMSE, consideration should be given to spectral features with greatest sensitivity to the extreme contributors, the dwarfs and giants. Two features selected for illustration are λ 4200 and λ 4226;

λ 4200 has a CN band as a principal contributor and is enhanced in giant stars, while λ 4226 has a Ca I line as a principal contributor and is enhanced in dwarf stars. Figure 6 illustrates the calculated values of equivalent width (Å) vs. the initial mass function exponent, n, for each of the four types of models. The observed equivalent width for the four galaxies is indicated. If the lower main sequence were dwarf enriched, λ 4226 would be greater than observed and λ 4200 less than observed. The model which best fits both features is obviously closer to n = -1 than any of the more dwarf enriched models; dwarf depleted models are also reasonable fits for NGC 3379 and 4472.

An immediate and important conclusion on age may be drawn from the statistical indicators AD and RMSE in Figures 2 through 5. The light from all four galaxies apparently arises from stars younger than an NGC 188 (or NGC 188 + M) cluster. The assumption in deriving this conclusion that only stars of a single age are present qualifies this result. Since our galaxy and the Magellanic Clouds are mixtures of stars of various ages, it appears reasonable that elliptical galaxies also consist of superpositions of populations of many ages. The light could be dominated by moderately old stars mixed with stars as old as NGC 188, which could still be present in significant numbers.

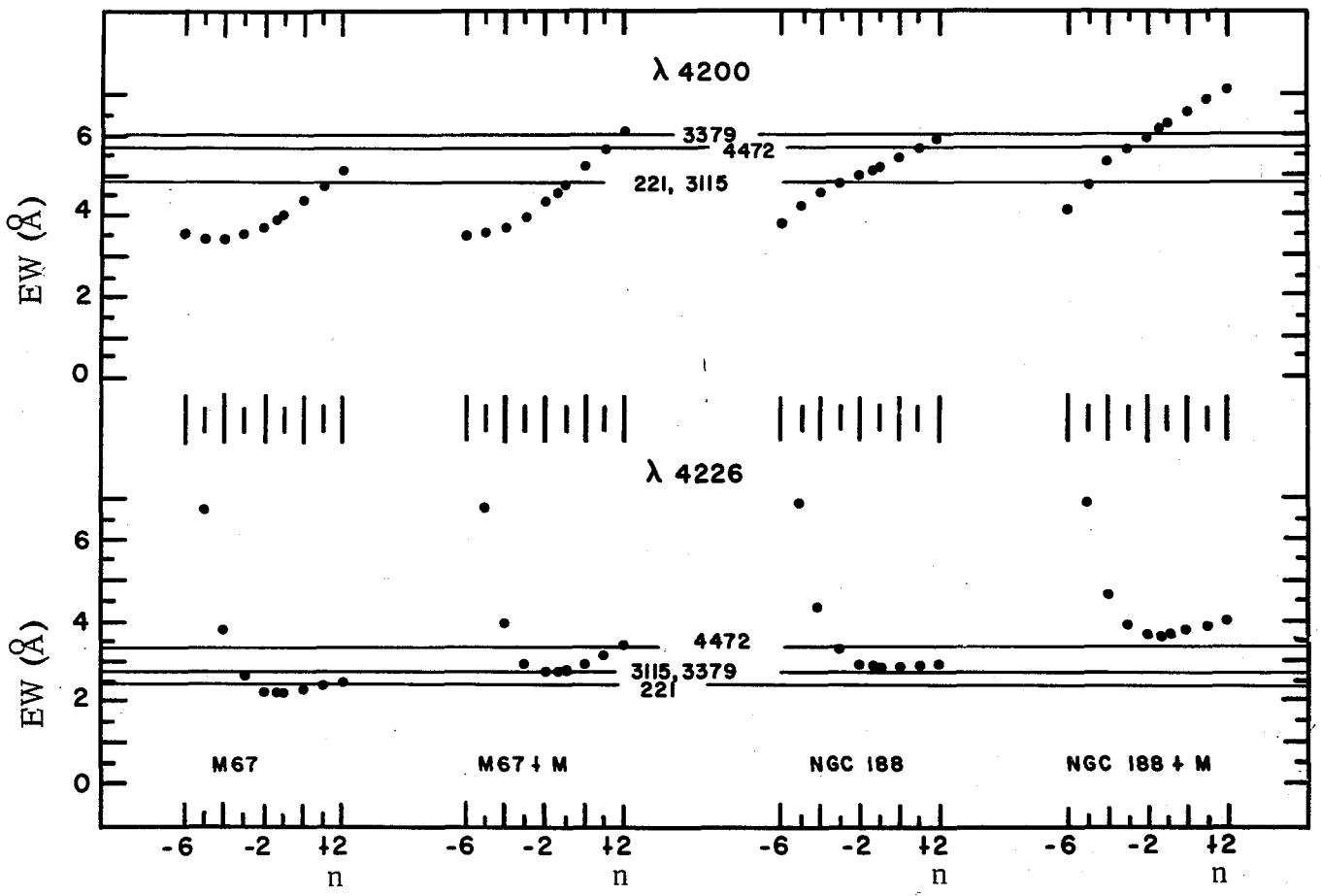

Fig. 6--Calculated and Observed Equivalent Widths (Å) vs. n for λ 4200 and λ 4226.

It would be desirable to extend this type of study to include superpositions of aggregates of various ages when sufficient data are available on evolutionary models. It appears that three of the four galaxies are well represented by an assemblage of stars resembling M67 enriched with M giants, but a younger assemblage than M67 appears to be necessary to represent the S0 galaxy NGC 3115.

The M/L ratios are plotted in Figure 7. Current observational values shown for the three ellipticals are from Fish (1964) and for the S0 from Limber (1960). For each galaxy the two intercepts correspond to a dwarf enriched model or to a dwarf depleted model. The intermediate mass elliptical NGC 3379 and giant elliptical NGC 4472 appear to be represented best on the dwarf depleted side of the curves. As already stated in an earlier equivalent width discussion, the differences in residuals near $n = -1.35$ are marginal even though RMSE is at a minimum near $+1$. In addition for M/L considerations the assumption that all the mass of the stars originally very bright on the main sequence is retained in the form of interstellar matter and white dwarfs forces an overestimate of M/L; it is probable that reddening of the nuclei would be much greater than observed if so much interstellar matter were to be retained. In contrast with the giant ellipticals,

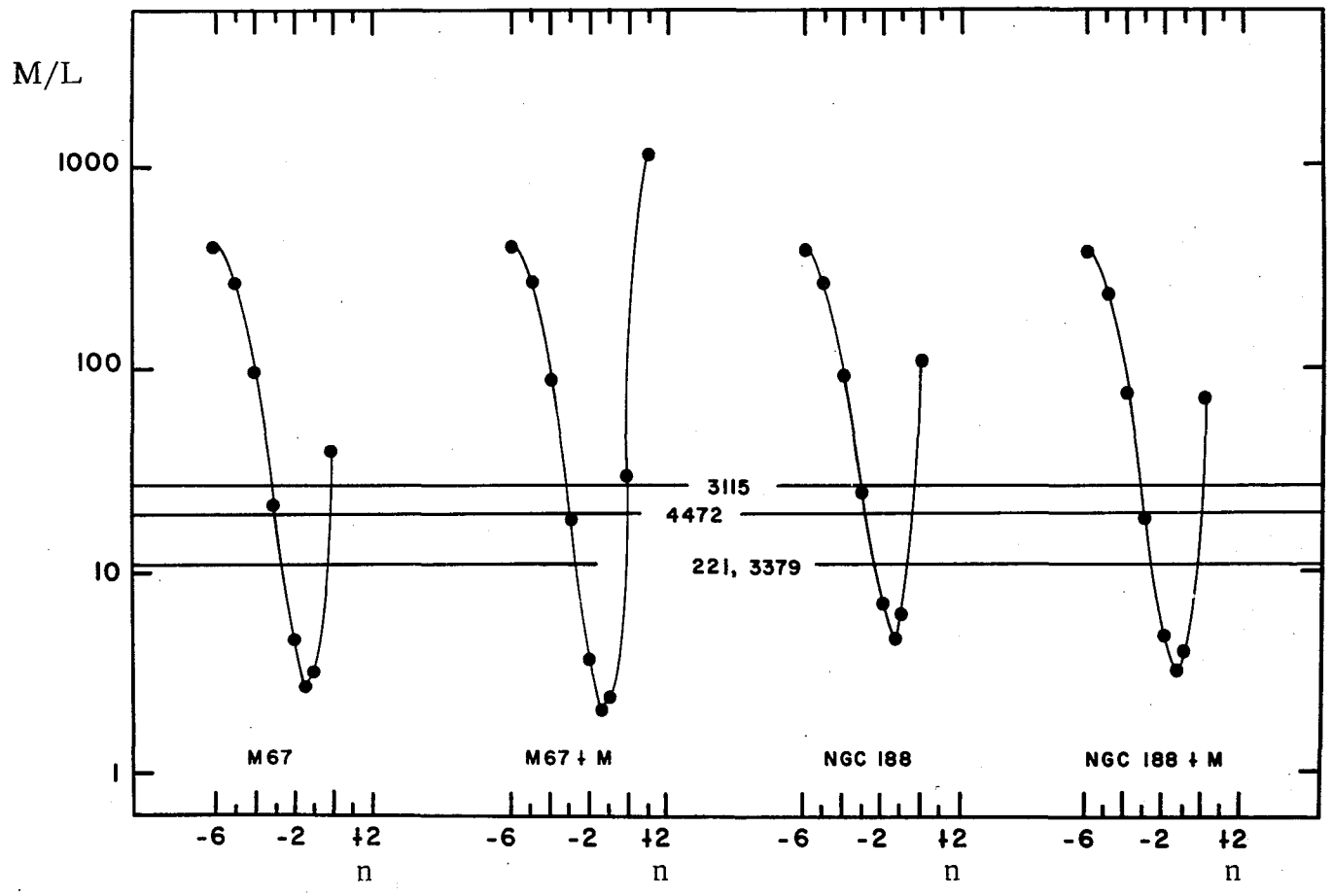

Fig. 7--M/L vs. n for M67, M67 + M, NGC 188, and NGC 188 + M.

the dwarf system M32 and S0 NGC 3115 have observed M/L too great to agree with the M/L calculated in the models at the best fit with observed equivalent widths. It was noted earlier that models of younger age than M67 are required to represent NGC 3115.

A measure of how well the best model represents the observations can be obtained by comparing the RMSE for the realistic model M67 + M, $n = -1.35$, with the root mean square of the internal standard deviation of the observed equivalent widths:

TABLE 16
Comparison of RMSE and Internal Standard Deviation

NGC	RMSE (Å)	INTERNAL (Å)
221	0.63	0.61
3115	0.57	0.51
3379	0.83	0.74
4472	0.84	0.73

The RMSE approaches the root mean square of the internal standard deviation of the observed equivalent widths closely; the minimum RMSE for NGC 3379 is 0.71 and for NGC 4472 is 0.76, which are marginally closer to the internal standard deviations.

The basic conclusions may be summarized as follows:

1. The initial luminosity function observed in our galaxy satisfactorily represents the equivalent widths of spectral features in elliptical galaxies. Dwarf enrichment is not likely for all four galaxies, but dwarf depletion may occur in the nuclei of the intermediate mass and giant elliptical studied. M/L ratios support the depletion hypothesis.

2. The light in all four galaxies appears to arise from aggregates younger than NGC 188, the oldest known cluster in our galaxy. Three of the four galaxies are well represented by light from a cluster like M67 augmented by M giants; the S0 NGC 3115 appears to require a younger model.

APPENDIX I
OBSERVATIONS AND REDUCTION PROCEDURES

The calibration of all stellar plates and most galaxy plates is accomplished as a part of the exposure at the telescope. A special decker with a clear central section and strips of Kodak neutral density filters near each end is placed at the spectrograph slit. The star or galaxy is then trailed repeatedly across the full length of the decker including filters; with this procedure the reductions include the effects of reciprocity failure and wavelength dependence of the plate characteristic curve, at the penalty of increased exposure time. The filters were calibrated near the beginning and end of the observing program, using the Cary Model 14 Recording Spectrophotometer located at the Kitt Peak National Observatory; the two measurements are in good agreement at all wavelengths. Projected slit width is 16 microns on all plates; projected slit length on stellar plates is approximately 1.3 mm. and on galaxy plates is approximately 0.5 mm.

The density tracings are made on the Hilger and Watts Model 471 Recording Microphotometer located at the

Steward Observatory. The portion of the spectrum from the clear portion of the slit is traced first in the usual way, then the plate is rotated 90^{o} and traced across the dispersion, without altering the densitometer settings, slit width, or slit length. Sampling is done at 100 Å intervals for stars and 50 Å intervals for galaxies.

Each tracing of star or galaxy is marked with continuum and feature limits by comparison with master tracings of an early and late type star. Each feature on the tracing is digitized by hand (using an IBM Port-A-Punch) at regular intervals corresponding to approximately three microns on the original plate. The intensity calibrations are also digitized. All cards for each plate are then reduced on the IBM 7072 computer of the Numerical Analysis Laboratory of the University of Arizona.

The computer program first reads the intensity calibration. At each sampled wavelength the calibrated densities of the filters and the measured densities of the spectrum are fitted to a simple curve. The next sampled wavelength is similarly treated until all are processed, then a least squares solution for the plate characteristic curve as a function of wavelength is performed. Next each feature is processed for equivalent width. The separation in Å of the sample points is read in, then the

densities of the pseudo-continuum and densities of the feature's sample points. These are converted to intensities within the computer and the equivalent width integrated using Simpson's rule. All input and computational results are printed out for inspection, with comments from the program if an error is suspected in the data. Velocity of the galaxy is neglected in the reduction since redshift has an entirely negligible effect on equivalent width for all galaxies observed.

The following Tables and Figures present the observational results. In Figure 8 are copies of a stellar (61 Cyg A) and a galaxy (M32) plate with microphotometer transmission tracings of the vicinity of the λ 4404 feature from these plates. Stellar results are listed in Table 6. Tabulated quantities are HD number, spectral type, B-V, and equivalent width (Å) for each feature. Galaxy results are listed in Table 7. Tabulated quantities are NGC number, equivalent widths (Å), standard deviations, number of plates on which width is based and root mean square internal standard deviation. Stellar equivalent widths (Å) are shown in Figures 9 through 16 as a function of B-V, where B-V is not corrected for reddening.

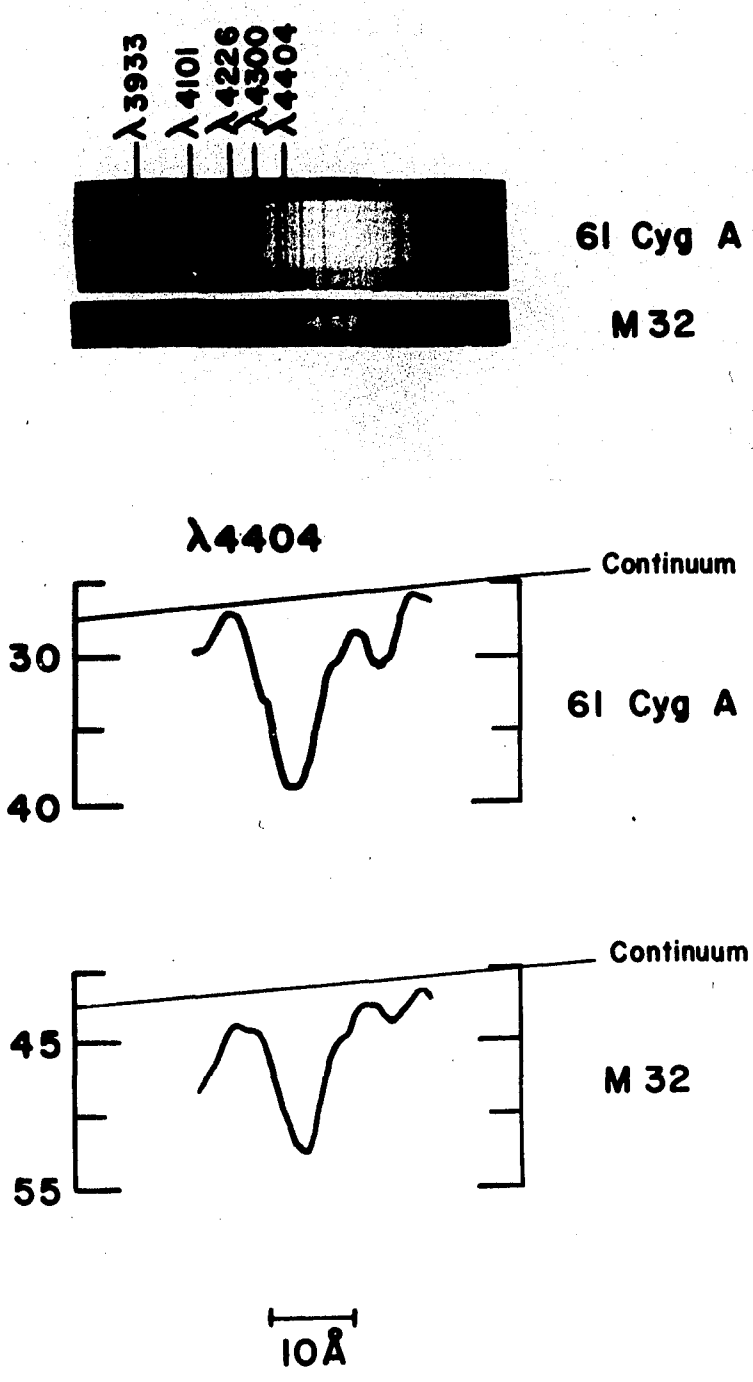

Fig. 8--Stellar and Galaxy Spectra with λ4404 Tracing.

TABLE 6
STELLAR OBSERVATIONAL DATA

H.D.	25291	17094	182835	164136	13174	21770	193370	195295	134083	220657
TYPE	F0 II	F0 IV	F2 Ib	F2 II	F2 III	F4 III	F5 Ib	F5 II	F5 V	F8 IV
B-V	0.49	0.31	0.60	0.39		0.42	0.65	0.40	0.43	0.61
4077	1.07	1.56	1.60	0.32	1.52	1.15	1.22	0.86	1.26	1.44
4101	5.76	7.59	5.07	4.89	5.70	4.68	2.59	4.29	3.03	2.47
4130	1.10	0.79	0.98	0.46	0.92	0.75	0.86		0.65	0.51
4175	1.00	1.24	2.15	0.72	1.29	1.16	1.02	0.91	0.86	1.40
4200	1.68	1.48	1.10	2.26		1.44	1.62	1.56	1.14	1.77
4226	0.61	0.94	0.77	1.55	0.64	0.36	0.66	0.50	1.21	0.76
4254	0.68	0.47	0.54	1.42			0.29	0.43	0.54	0.78
4275	0.59	0.33	0.43	1.20	0.83	0.48	0.31		0.66	0.90
4289	0.86	1.09	0.88	1.81	0.94	0.65	1.22	0.73	1.37	1.40
4300	2.83	2.79	3.67	3.96	2.34	2.50	2.46	2.62	4.40	4.71
4340	6.40	6.41	5.44	5.93	5.05	3.93	2.50	4.67	2.62	2.46
4385	1.04	0.78	1.14	1.44	0.36	0.44	1.04	0.58	1.22	1.00
4404				0.72		0.41	0.86	1.30	0.52	0.53

TABLE 6—Continued

H.D.	9826	185758	150680	192713	159181	206859	173764	161797	186427	135722
TYPE	F8 V	G0 II	G0 IV	G2 Ib	G2 II	G5 Ib	G5 II	G5 IV	G5 V	G8 III
B-V	0.54	0.77	0.64	1.04	1.00	1.18	1.09	0.75	0.66	0.96
4077	1.22	1.74	1.31	2.36	1.43	1.49	2.39	1.90	1.56	2.46
4101	3.10	1.96	2.41	3.55	1.27	2.04	3.43	2.00	2.69	1.89
4130	0.62	1.08	0.52	2.82	1.13	2.03	1.82	1.25	0.93	2.05
4175	0.46	2.27	0.96	4.70	2.56	5.31	4.06	1.96	1.84	3.51
4200	1.20	3.36	2.74	6.26	2.84	5.96	5.84	3.58	4.20	4.75
4226	0.94	1.28	1.24	1.80	1.15	1.34	1.55	1.52	2.26	2.13
4254	0.30	0.68	1.43	1.94	0.98	0.92	1.18	1.27	2.04	1.92
4275	0.42	1.02	1.55	1.56	0.81	0.96	1.44	2.04	2.07	1.52
4289	1.04	1.79	1.63	2.36	1.74	1.90	1.95	2.13	2.14	2.54
4300	3.96	5.73	6.79	7.29	5.98	6.57	6.65	7.49	8.10	7.08
4340	2.47	1.84	2.17	2.65	1.41	0.95	2.32	1.82	2.40	1.29
4385	0.77	1.64	1.58		1.72	2.25	1.81	2.56	2.51	2.81
4404	0.48	0.81	0.98	1.34	1.10	1.38	1.22	1.62	1.37	1.39

TABLE 6—Continued

H.D.	188512	180809	145328	23249	3651	210745	163770	206778	153210	156283
TYPE	G8 IV	K0 II	K0 III	K0 IV	K0 V	K1 Ib	K1 II	K2 Ib	K2 III	K3 II
B-V	0.86	1.25	1.02	0.92	0.86	1.55	1.35	1.58	1.16	1.44
4077	2.27	3.27	2.44	2.50	1.86	3.33	3.95	2.35	2.67	4.08
4101	2.54	2.10	2.14	2.56	2.00	2.95	2.91	2.61	1.41	2.41
4130	1.46		2.50	2.12	1.90	3.64	5.05	3.13	2.17	4.82
4175	2.07	6.39	3.50	3.81	3.20	6.20	8.15	5.34	4.04	7.70
4200	4.18	8.27	7.43	5.24	7.15	9.19	13.02	5.32	9.39	7.87
4226	2.27	2.82	3.07	2.83	3.95	2.77	4.00	3.55	3.00	6.47
4254	1.97	1.84	2.14	2.38	2.99	2.25	3.22	2.40	1.94	4.50
4275	2.34	1.94	2.68	2.97	2.90	2.36	3.52	3.06	2.48	3.72
4289	2.35	2.86	2.57	2.62	3.06	3.59	3.65	3.99	2.50	
4300	7.87	7.59	8.66	8.68	9.11	5.77	9.43	6.07	8.35	11.38
4340	1.29	1.15	1.37	1.42	1.66	1.42	2.22	1.86	0.83	3.83
4385	2.76	3.12	3.17	3.32	3.73	2.81	4.01	3.25	3.40	7.10
4404	1.77	2.10	2.11	2.81	2.61	2.15	2.63	2.69	2.82	4.90

TABLE 6—Concluded

H.D.	127665	219134	120477	201091	201092	147379	141477	145713	156014
TYPE	K3 III	K3 V	K5 III	K5 V	K7 V	M0 V	M1 III	M4 III	M5 II
B-V	1.30	1.01	1.52	1.19	1.38	1.41	1.60		1.45
4077	3.14	2.20	6.13	2.58	2.68	2.98	3.86	2.84	2.53
4101	3.13	2.04	4.85	2.38	3.19	1.21	2.69	2.46	2.11
4130	3.50	2.16	4.48	1.95	2.20	1.11	2.19	2.12	2.46
4175	4.36	2.91	6.02	2.88	2.59	1.56	3.93	1.93	2.18
4200	10.01	5.53	10.39	5.70	5.20	3.71	7.29	4.69	4.68
4226	4.36	4.80	7.95	8.96	9.72	10.66	6.74	7.69	7.28
4254	2.72	3.75	4.17	3.93	5.09	5.37	3.09		3.09
4275	3.43	3.77	4.91	4.22	3.81	4.82	3.18		2.96
4289	3.43	3.17	4.20	4.33	3.68	3.34	4.07		2.52
4300	9.24	8.50	8.11	7.41	5.66	7.40	6.61		6.37
4340	1.19	1.24	1.05	1.48	0.75	0.44			1.74
4385	4.09	6.34	4.14	4.06	3.30	3.33			1.67
4404	3.17	2.92	3.20	2.70	1.47	1.73			1.90

TABLE 7
GALAXY OBSERVATIONAL DATA

NGC	221			3115			3379			4472		
Feature	EW		n	EW		n	EW		n	EW		n
4077	1.34	0.18	4	1.34	0.49	3	2.10	1.48	3	1.18	0.56	3
4101	3.45	0.53	4	2.58	0.22	3	2.40	0.27	3	2.52	0.87	3
4130	1.70	0.47	4	1.36	0.58	3	1.48	0.79	3	2.27	0.95	3
4175	2.43	0.68	4	1.92	0.75	3	2.96	0.48	3	3.09	0.13	3
4200	4.78	1.32	4	4.79	0.34	3	6.06	1.46	3	5.70	1.29	3
4226	2.37	0.38	4	2.73	0.26	3	2.74	0.50	3	3.33	0.43	3
4254	1.66	0.64	4	1.25	0.50	3	1.96	0.66	3	1.50	0.19	3
4275	2.02	0.50	4	1.92	0.39	3	2.31	0.43	3	2.13	0.61	3
4289	2.51	0.46	4	1.95	0.36	3	3.08	0.35	3	2.58	1.00	3
4300	6.63	0.64	4	6.54	0.24	3	6.77	0.62	3	6.68	1.16	3
4340	2.08	0.41	4	1.22	0.30	3	0.90	0.17	3	1.01	0.54	3
4385	2.90	0.39	4	2.54	1.06	3	2.94	0.67	3	2.64	0.18	3
4404	1.78	0.59	4	1.31	0.46	3	1.56	0.16	3	1.24	0.04	3
RMS Internal		0.61			0.51			0.74			0.73	

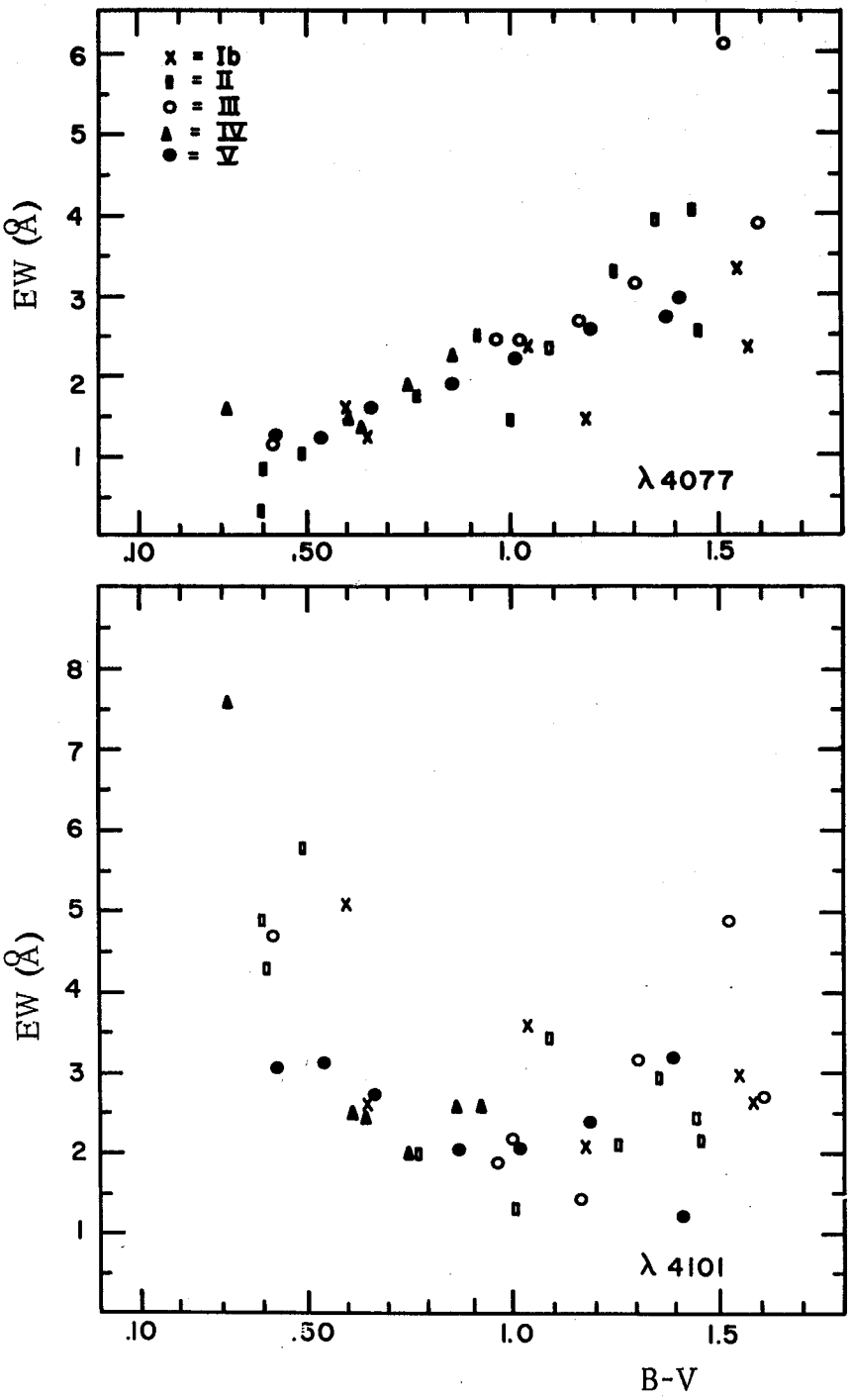

Fig. 9--Equivalent Widths (Å) vs. B-V for λ 4077 and λ 4101

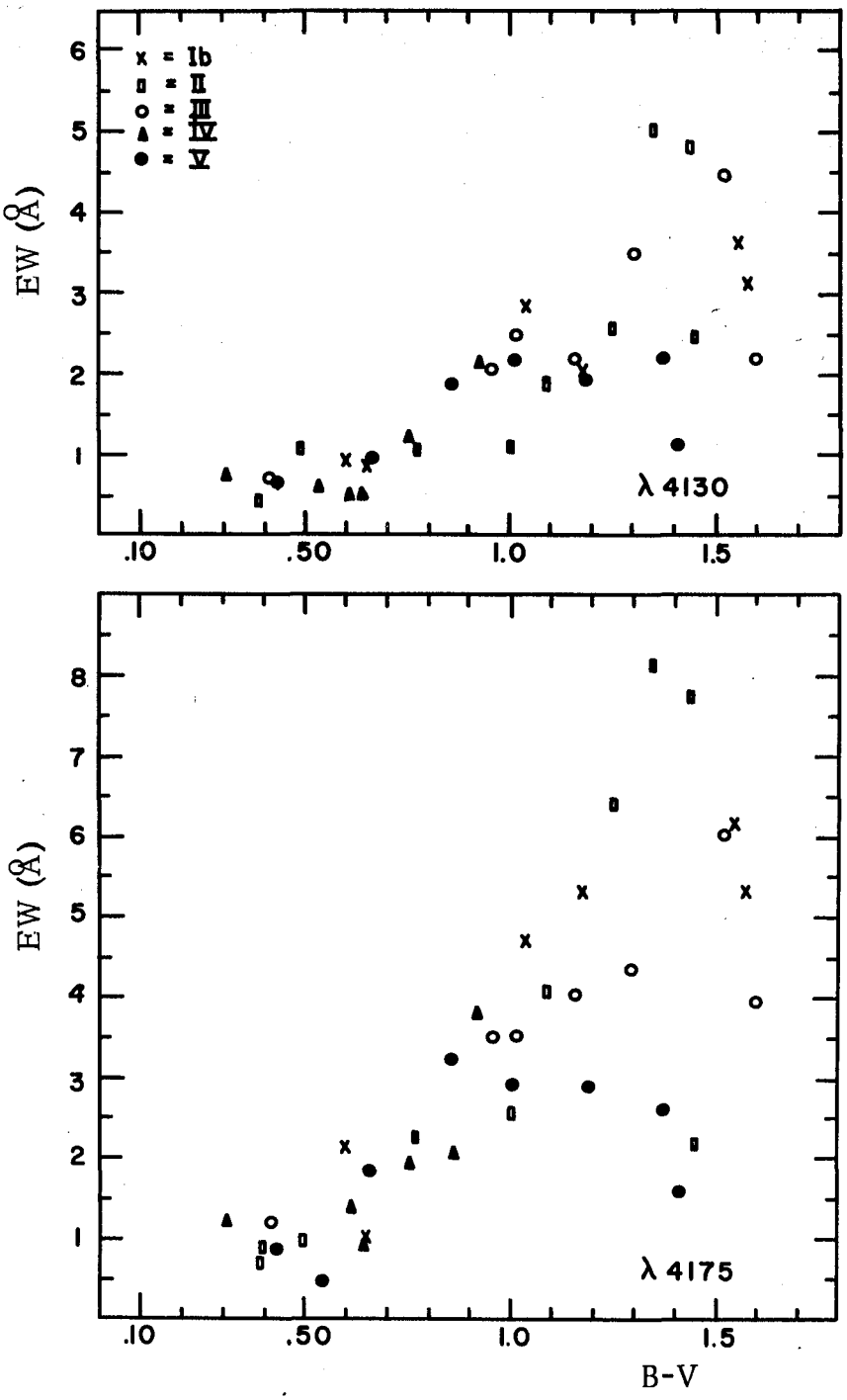

Fig. 10--Equivalent Widths (Å) vs. B-V for λ 4130 and λ 4175.

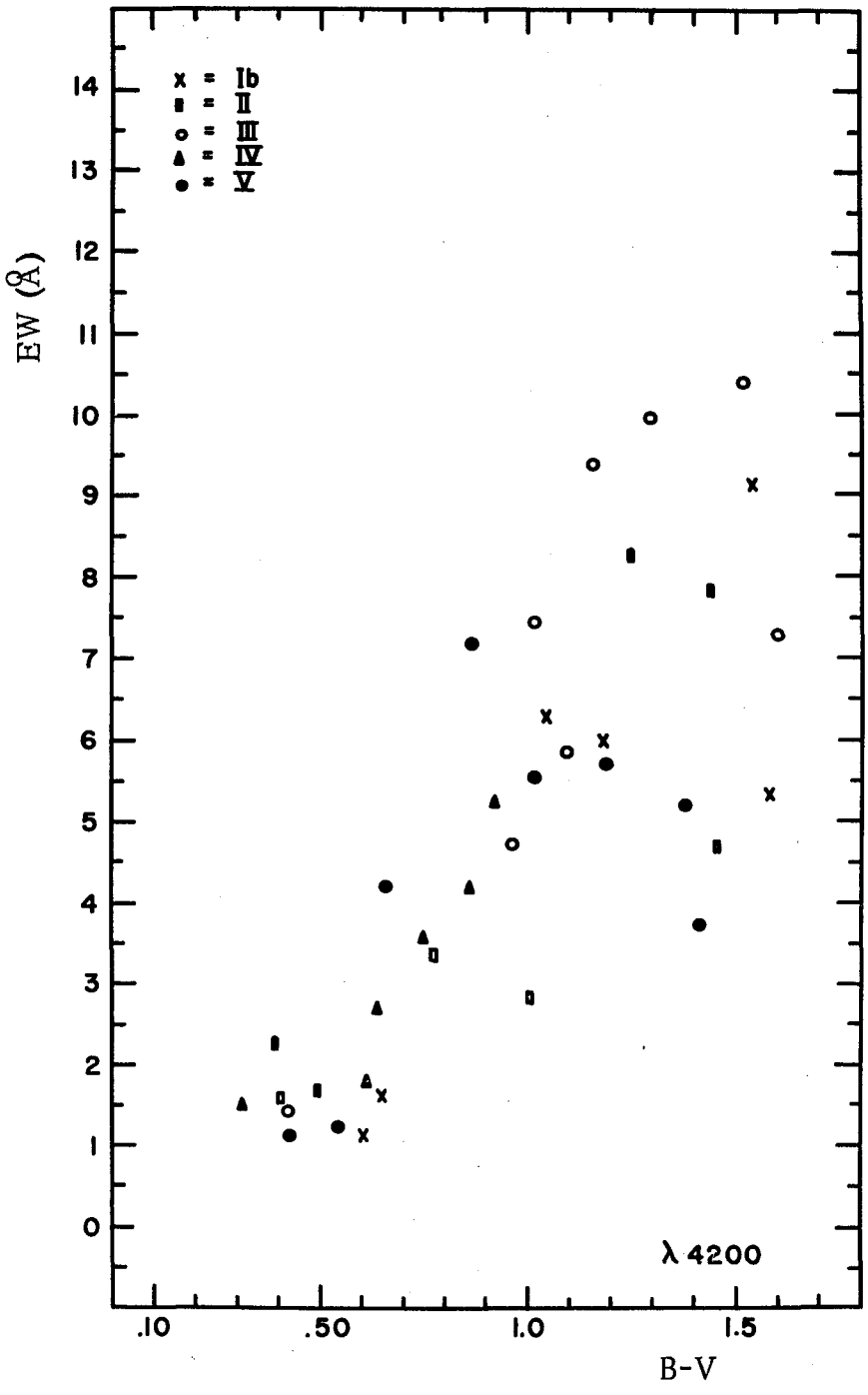

Fig. 11--Equivalent Widths (Å) vs. B-V for λ 4200.

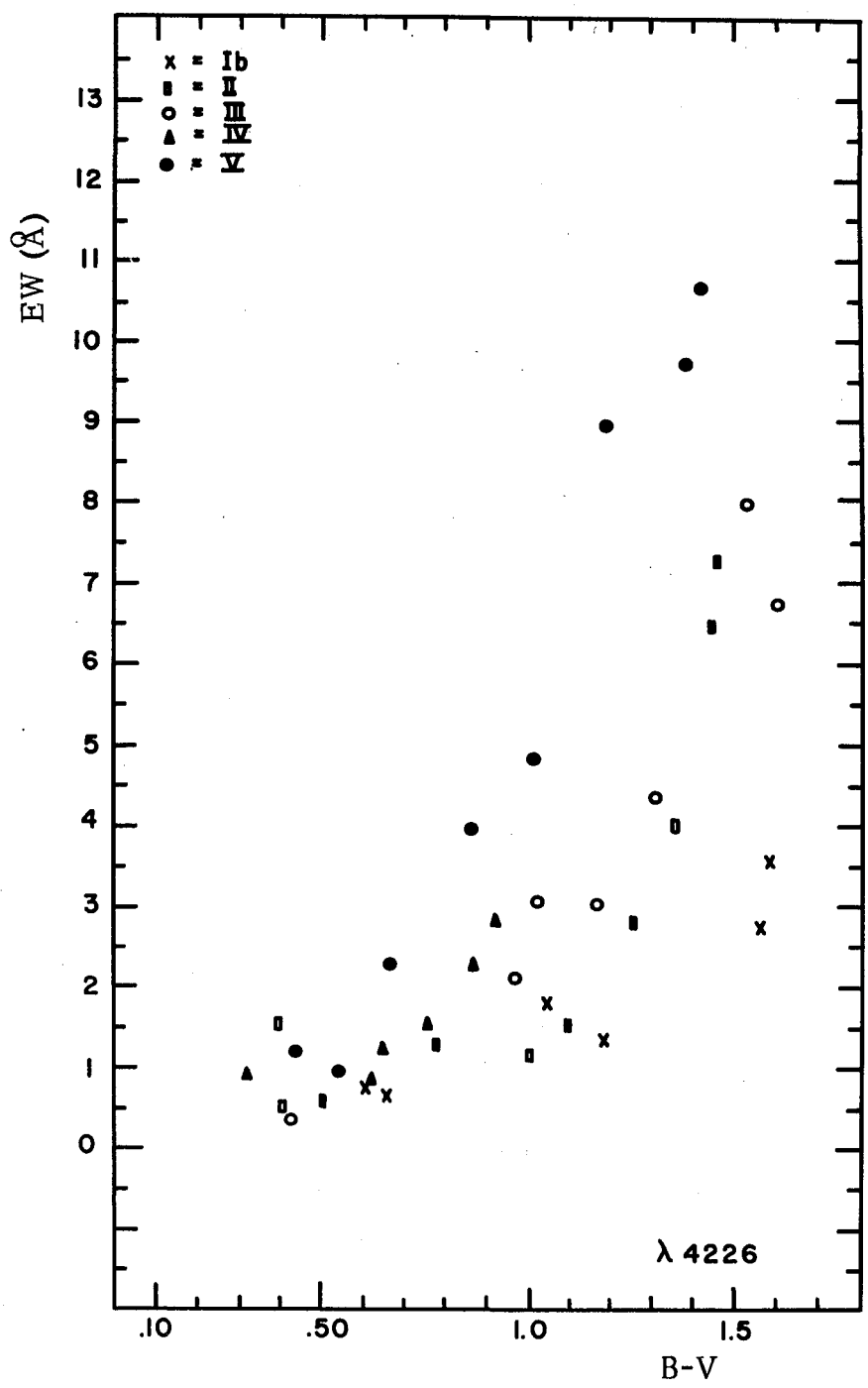

Fig. 12--Equivalent Widths (Å) vs. B-V for λ 4226.

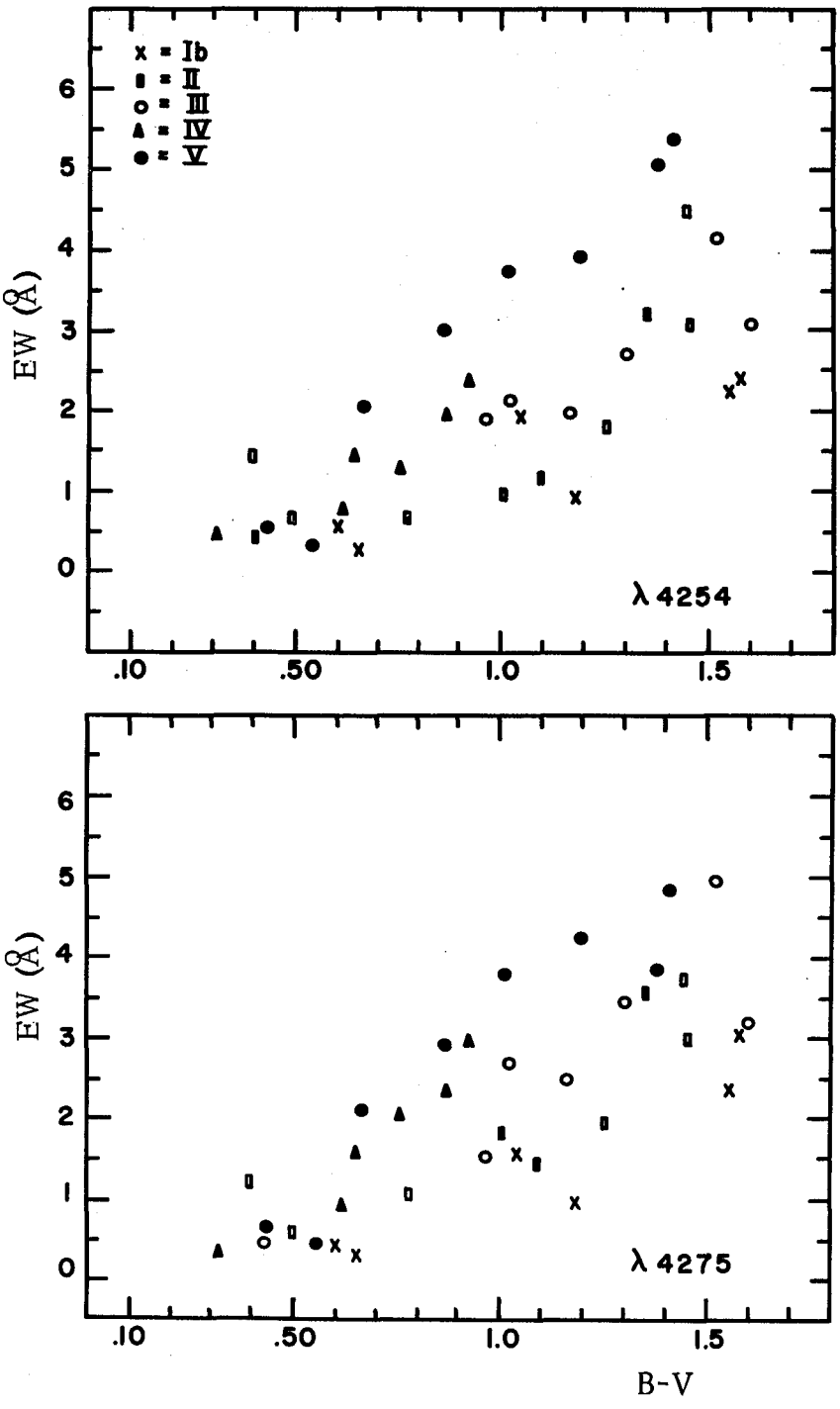

Fig. 13--Equivalent Widths (Å) vs. B-V for λ 4254 and λ 4275.

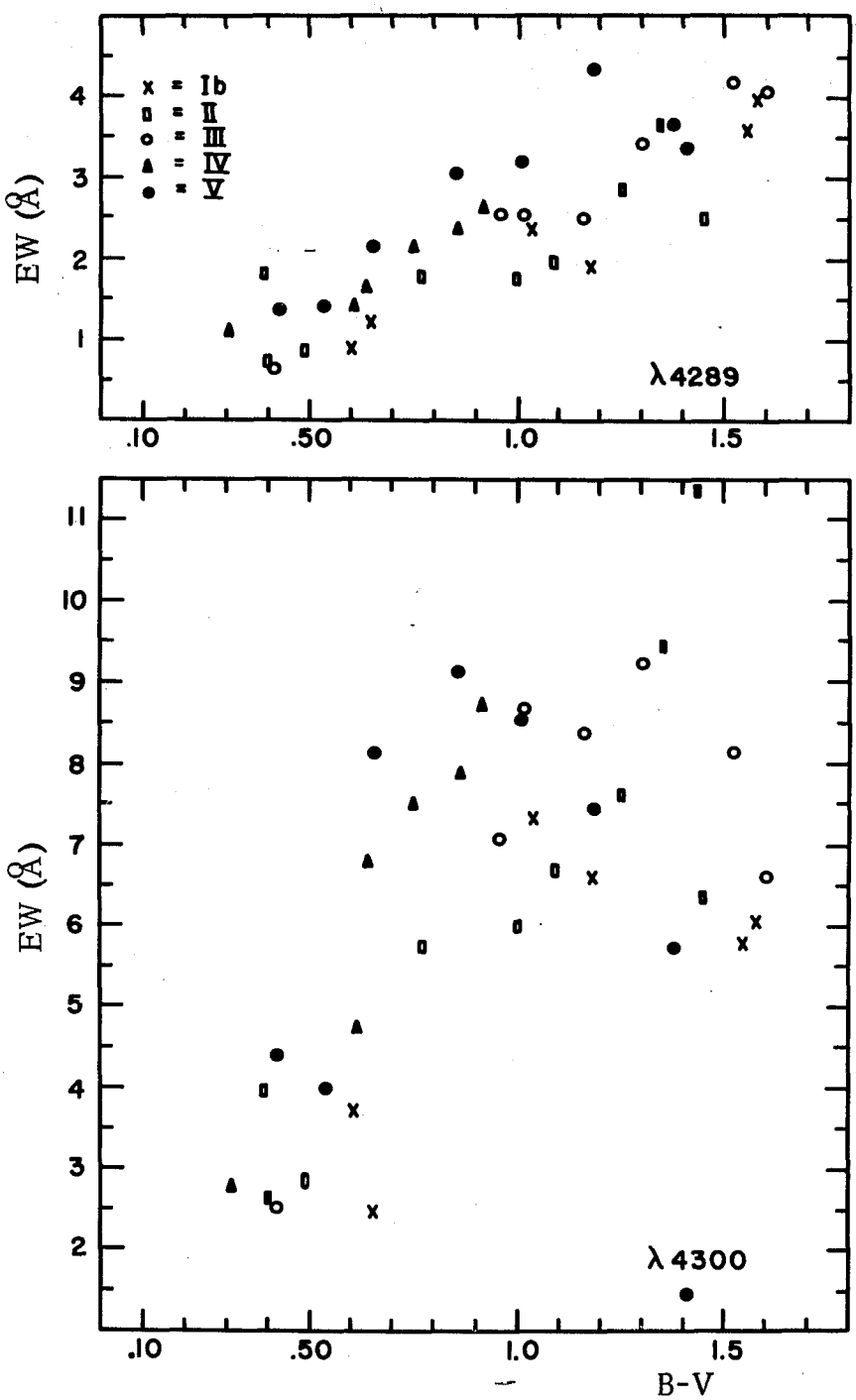

Fig. 14--Equivalent Widths (Å) vs. B-V for λ 4289 and λ 4300.

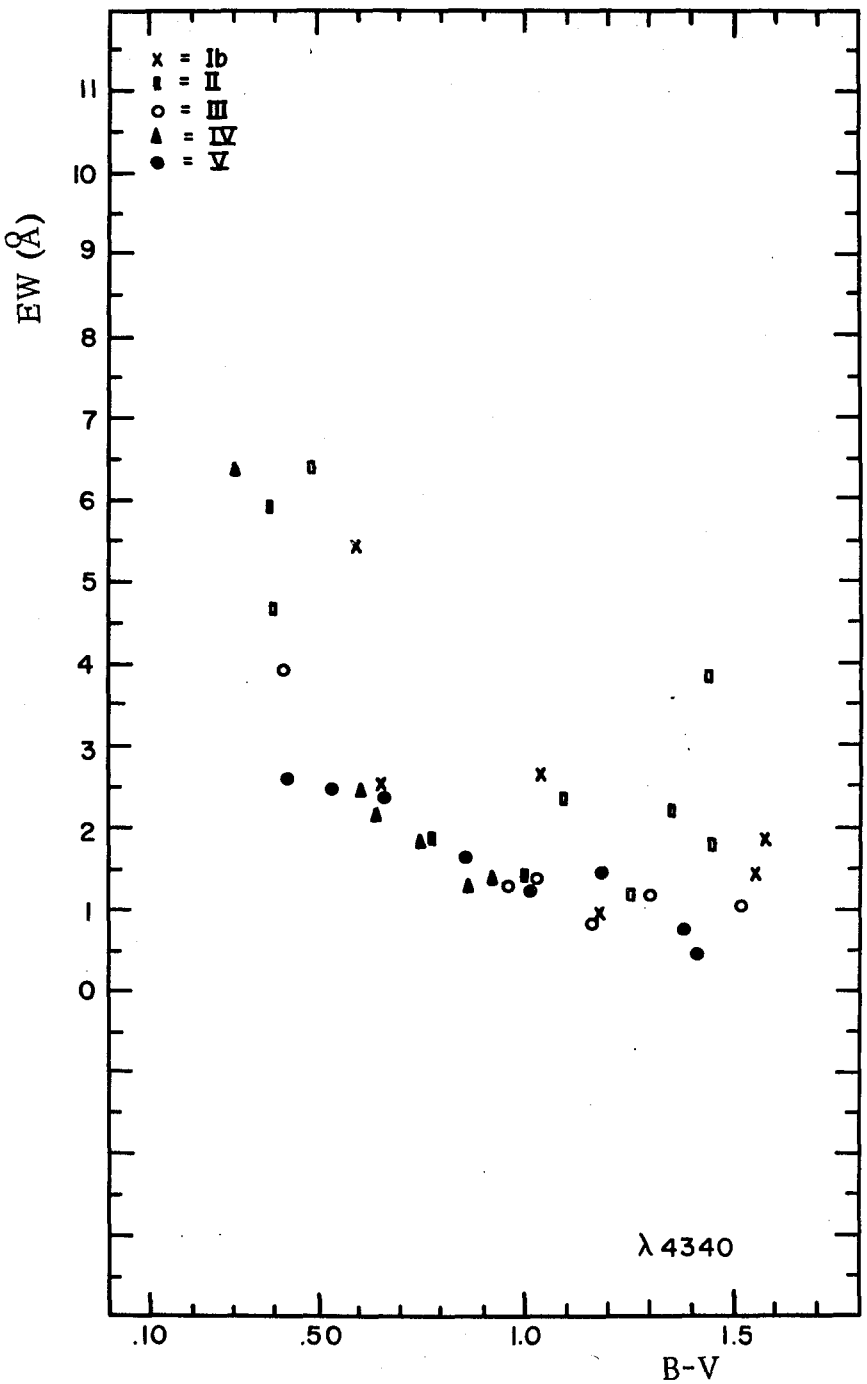

Fig. 15--Equivalent Widths (Å) vs. B-V for λ 4340.

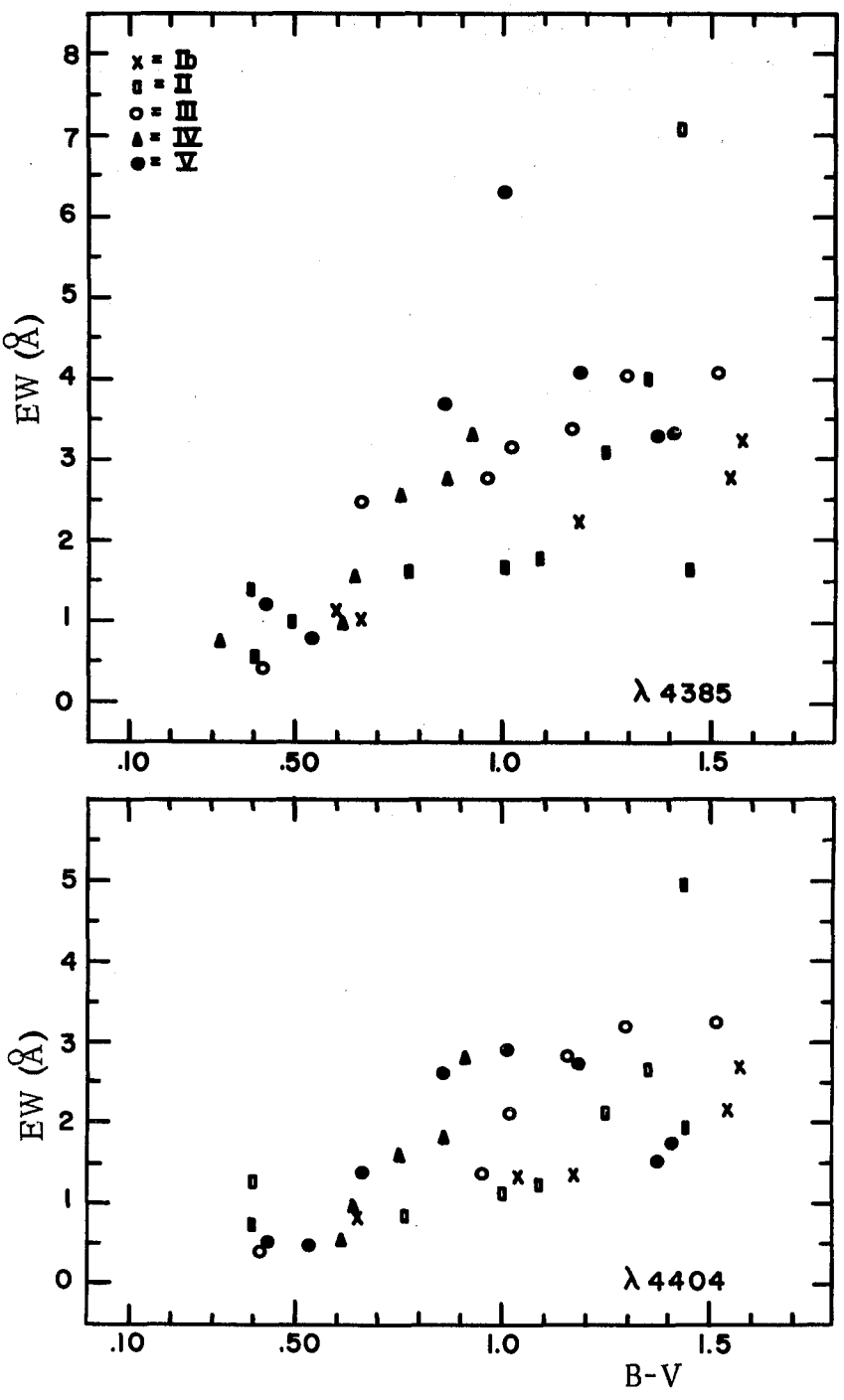

Fig. 16--Equivalent Widths (Å) vs. B-V for λ 4385 and λ 4404.

APPENDIX II
THEORETICAL RESULTS AND STATISTICAL TABULATIONS

The results of the model calculations and comparisons with observations for each of the models M67, M67 + M, NGC 188, and NGC 188 + M are listed in Tables 8 through 15. The value of the power law exponent, n, is listed across the top of the page and applies to all quantities below it. Down the side of the page are listed: (1) the designations of the spectral features used, followed by the calculated equivalent widths (Å); (2) the M/L ratios (in solar units); (3) the average deviation (AD) defined in the text (Å); and, (4) the root mean square error (RMSE) defined in the text (Å).

TABLE 8
M67 MODEL RESULTS

Feature \ n	2	1	0	-1	-1.35	-2	-3	-4	-5	-6
4077	2.00	1.92	1.84	1.77	1.74	1.71	1.70	1.80	2.18	2.68
4101	2.51	2.57	2.64	2.69	2.71	2.73	2.73	2.66	2.44	2.19
4130	1.68	1.56	1.44	1.32	1.29	1.23	1.17	1.20	1.38	1.61
4175	2.59	2.43	2.27	2.12	2.06	1.98	1.87	1.80	1.73	1.64
4200	5.08	4.74	4.38	4.04	3.93	3.74	3.53	3.43	3.46	3.50
4226	2.47	2.35	2.25	2.20	2.20	2.25	2.57	3.73	6.75	10.03
4254	1.91	1.84	1.77	1.73	1.73	1.75	1.89	2.39	3.64	4.93
4275	2.12	2.04	1.97	1.91	1.90	1.90	2.00	2.38	3.33	4.30
4289	2.39	2.31	2.22	2.15	2.13	2.11	2.11	2.22	2.47	2.68
4300	7.40	7.28	7.17	7.06	7.03	6.98	6.85	6.45	5.19	3.75
4340	1.72	1.81	1.90	1.98	2.00	2.03	2.02	1.83	1.30	0.78
4385	2.78	2.68	2.58	2.49	2.46	2.43	2.42	2.47	2.55	2.54
4404	1.88	1.77	1.66	1.55	1.52	1.46	1.39	1.29	1.00	0.69
M/L	86,000.	1,700.	41.	3.1	2.7	4.6	21.	96.	270.	390.

TABLE 9
M67+M MODEL RESULTS

Feature \ n	2	1	0	-1	-1.35	-2	-3	-4	-5	-6
4077	2.23	2.13	2.03	1.93	1.89	1.84	1.79	1.86	2.20	2.68
4101	2.43	2.50	2.56	2.63	2.65	2.68	2.69	2.64	2.44	2.18
4130	2.08	1.92	1.76	1.60	1.54	1.45	1.33	1.30	1.43	1.62
4175	2.97	2.79	2.59	2.40	2.33	2.21	2.04	1.91	1.78	1.65
4200	6.05	5.63	5.19	4.74	4.59	4.32	3.96	3.71	3.59	3.53
4226	3.39	3.17	2.97	2.79	2.75	2.71	2.89	3.88	6.76	10.02
4254	2.24	2.14	2.04	1.96	1.94	1.93	2.01	2.44	3.64	4.92
4275	2.36	2.26	2.17	2.08	2.06	2.04	2.09	2.42	3.33	4.29
4289	2.72	2.62	2.50	2.39	2.36	2.30	2.25	2.30	2.50	2.69
4300	7.34	7.25	7.15	7.07	7.04	6.99	6.87	6.47	5.23	3.77
4340	1.45	1.55	1.66	1.77	1.80	1.86	1.90	1.76	1.28	0.78
4385	3.15	3.02	2.90	2.77	2.73	2.66	2.59	2.58	2.59	2.55
4404	2.18	2.06	1.93	1.80	1.75	1.67	1.55	1.39	1.05	0.71
M/L	56,000.	1,150.	29.	2.3	2.0	3.6	18.	87.	270.	389.

TABLE 10
NGC 188 MODEL RESULTS

Feature \ n	2	1	0	-1	-1.35	-2	-3	-4	-5	-6
4077	2.19	2.14	2.09	2.04	2.03	2.01	2.01	2.09	2.35	2.72
4101	2.29	2.32	2.34	2.37	2.37	2.38	2.38	2.35	2.25	2.12
4130	1.96	1.88	1.80	1.72	1.70	1.66	1.61	1.60	1.63	1.70
4175	2.93	2.83	2.73	2.63	2.60	2.54	2.44	2.31	2.06	1.79
4200	5.87	5.63	5.39	5.16	5.09	4.96	4.76	4.53	4.16	3.79
4226	2.91	2.85	2.82	2.83	2.85	2.94	3.29	4.33	6.90	9.83
4254	2.21	2.18	2.16	2.16	2.17	2.21	2.35	2.77	3.77	4.88
4275	2.42	2.38	2.36	2.35	2.36	2.38	2.48	2.79	3.51	4.29
4289	2.62	2.57	2.53	2.50	2.49	2.48	2.49	2.54	2.64	2.73
4300	8.02	7.97	7.92	7.86	7.84	7.78	7.60	7.05	5.63	4.03
4340	1.50	1.55	1.60	1.64	1.65	1.66	1.64	1.50	1.14	0.76
4385	3.11	3.05	3.01	2.97	2.96	2.94	2.92	2.88	2.76	2.62
4404	2.18	2.12	2.06	2.00	1.98	1.95	1.87	1.68	1.24	0.80
M/L	460,000.	6,400.	109.	6.0	4.6	6.7	24.	91.	260.	380.

TABLE 11

NGC 188 + M MODEL RESULTS

Feature \ n	2	1	0	-1	-1.35	-2	-3	-4	-5	-6
4077	2.46	2.39	2.32	2.25	2.23	2.20	2.17	2.20	2.41	2.73
4101	2.23	2.26	2.29	2.31	2.32	2.33	2.34	2.32	2.24	2.12
4130	2.42	2.31	2.20	2.09	2.06	1.99	1.90	1.82	1.77	1.75
4175	3.35	3.23	3.11	2.98	2.94	2.86	2.72	2.54	2.22	1.86
4200	6.94	6.65	6.36	6.06	5.96	5.77	5.47	5.10	4.53	3.95
4226	3.99	3.85	3.73	3.64	3.62	3.63	3.83	4.64	6.94	9.77
4254	2.57	2.51	2.47	2.44	2.43	2.44	2.53	2.87	3.77	4.85
4275	2.65	2.60	2.56	2.53	2.53	2.53	2.60	2.84	3.50	4.26
4289	2.99	2.92	2.86	2.80	2.78	2.75	2.71	2.70	2.73	2.76
4300	7.78	7.76	7.74	7.72	7.70	7.67	7.53	7.05	5.72	4.10
4340	1.22	1.28	1.34	1.39	1.41	1.44	1.46	1.38	1.09	0.75
4385	3.47	3.40	3.34	3.27	3.25	3.21	3.15	3.06	2.87	2.67
4404	2.47	2.41	2.34	2.26	2.24	2.19	2.08	1.87	1.38	0.86
M/L	275,000.	4,000.	70.	4.0	3.2	4.7	18.	75.	230.	370.

TABLE 12

M67 OBSERVATIONAL AVERAGE DEVIATION (AD)

NGC \ n	2	1	0	-1	-1.35	-2	-3	-4	-5	-6
221	-0.07	0.03	0.12	0.20	0.23	0.26	0.26	0.15	-0.14	-0.44
3115	-0.39	-0.30	-0.20	-0.12	-0.10	-0.06	-0.06	-0.17	-0.46	-0.76
3379	0.06	0.15	0.24	0.33	0.35	0.38	0.38	0.28	-0.01	-0.31
4472	-0.05	0.04	0.14	0.22	0.24	0.28	0.28	0.17	-0.12	-0.42

M67 OBSERVATIONAL ROOT MEAN SQUARE ERROR (RMSE)

NGC \ n	2	1	0	-1	-1.35	-2	-3	-4	-5	-6
221	0.68	0.64	0.64	0.67	0.68	0.70	0.74	0.88	1.66	2.71
3115	0.65	0.60	0.58	0.59	0.60	0.62	0.64	0.75	1.54	2.59
3379	0.77	0.82	0.90	0.98	1.01	1.05	1.08	1.12	1.67	2.62
4472	0.82	0.85	0.91	0.98	1.00	1.03	1.05	1.07	1.60	2.55

TABLE 13

M67 + M OBSERVATIONAL AVERAGE DEVIATION (AD)

NGC \ n	2	1	0	-1	-1.35	-2	-3	-4	-5	-6
221	-0.38	-0.26	-0.14	-0.02	0.02	0.08	0.13	0.08	-0.17	-0.44
3115	-0.70	-0.58	-0.46	-0.34	-0.31	-0.25	-0.19	-0.25	-0.49	-0.77
3379	-0.26	-0.14	-0.01	0.10	0.14	0.20	0.25	0.20	-0.04	-0.32
4472	-0.36	-0.24	-0.12	0.00	0.03	0.09	0.15	0.09	-0.15	-0.43

M67 + M OBSERVATIONAL ROOT MEAN SQUARE ERROR (RMSE)

NGC \ n	2	1	0	-1	-1.35	-2	-3	-4	-5	-6
221	0.89	0.77	0.69	0.64	0.63	0.64	0.68	0.86	1.65	2.70
3115	0.89	0.76	0.66	0.59	0.57	0.57	0.59	0.74	1.53	2.59
3379	0.72	0.71	0.73	0.80	0.83	0.89	0.96	1.06	1.65	2.62
4472	0.80	0.76	0.77	0.82	0.84	0.88	0.94	1.01	1.58	2.54

TABLE 14

NGC 188 OBSERVATIONAL AVERAGE DEVIATION (AD)

NGC \ n	2	1	0	-1	-1.35	-2	-3	-4	-5	-6
221	-0.35	-0.29	-0.24	-0.20	-0.19	-0.17	-0.17	-0.21	-0.34	-0.49
3115	-0.67	-0.62	-0.56	-0.52	-0.51	-0.49	-0.49	-0.53	-0.66	-0.82
3379	-0.23	-0.17	-0.12	-0.08	-0.06	-0.05	-0.04	-0.09	-0.22	-0.37
4472	-0.33	-0.28	-0.22	-0.18	-0.17	-0.15	-0.15	-0.19	-0.32	-0.48

NGC 188 OBSERVATIONAL ROOT MEAN SQUARE ERROR (RMSE)

NGC \ n	2	1	0	-1	-1.35	-2	-3	-4	-5	-6
221	0.90	0.85	0.81	0.78	0.77	0.76	0.78	0.95	1.66	2.62
3115	0.90	0.85	0.80	0.76	0.75	0.73	0.73	0.86	1.56	2.51
3379	0.77	0.76	0.77	0.79	0.79	0.80	0.83	0.95	1.59	2.52
4472	0.86	0.85	0.85	0.85	0.85	0.86	0.86	0.94	1.54	2.46

TABLE 15

NGC 188 + M OBSERVATIONAL AVERAGE DEVIATION (AD)

NGC \ n	2	1	0	-1	-1.35	-2	-3	-4	-5	-6
221	-0.68	-0.61	-0.54	-0.47	-0.45	-0.41	-0.37	-0.36	-0.42	-0.52
3115	-1.01	-0.93	-0.86	-0.79	-0.77	-0.73	-0.69	-0.69	-0.75	-0.85
3379	-0.56	-0.49	-0.41	-0.35	-0.32	-0.29	-0.25	-0.24	-0.30	-0.40
4472	-0.67	-0.59	-0.52	-0.45	-0.43	-0.39	-0.35	-0.35	-0.41	-0.51

NGC 188 + M OBSERVATIONAL ROOT MEAN SQUARE ERROR (RMSE)

NGC \ n	2	1	0	-1	-1.35	-2	-3	-4	-5	-6
221	1.22	1.13	1.05	0.98	0.96	0.93	0.91	1.03	1.66	2.59
3115	1.24	1.15	1.06	0.98	0.96	0.92	0.89	0.97	1.56	2.49
3379	0.92	0.86	0.82	0.79	0.78	0.78	0.80	0.93	1.56	2.48
4472	1.02	0.96	0.91	0.87	0.86	0.85	0.85	0.94	1.51	2.42

LIST OF REFERENCES

Allen, C. W. 1963, Astrophysical Quantities, (London: Athlone Press).

Arny, T. T. 1965, PhD Dissertation, Univ. of Arizona.

Baade, W. 1944, Ap. J., 100, 137.

Baum, W. A. 1959a, Ann. d. Astr., Supp., Fasc. No. 8.

Baum, W. A. 1959b, P. A. S. P., 71, 106.

Carpenter, E. F. 1963, A. J., 68, 275.

Cross, B. 1966, private communication.

Demarque, P. R., and Larson, R. B. 1964, Ap. J., 140, 544.

de Vaucouleurs, G., and de Vaucouleurs, A. 1958, Lowell Obs. Bull., 92.

de Vaucouleurs, G., and de Vaucouleurs, A. 1964, Reference Catalog of Bright Galaxies (Austin: Univ. of Texas Press).

Eggen, O. J., and Sandage, A. R. 1964, Ap. J., 140, 130.

Fehrenbach, C. 1958, Handbuch Der Physik, Vol. 50, (Berlin, Gottingen, Heidelberg: Pub. Springer-Verlag OHG).

Fish, R. A. 1964, Ap. J., 139, 284.

Gass, S. I. 1964, Linear Programming: Methods and Applications, 2 ed., (New York: McGraw-Hill Book Co.)

Greenstein, J. L., and Keenan, P. C. 1964, Ap. J., 140, 673.

Hallgren, E. L., and Demarque, P. R. 1966, Ap. J., 146, 430.

Holmberg, E. 1953, Medd. Lund Astr. Obs. Ser I, No. 180.

Hubble, E., and Humason, M. L. 1931, Ap. J., 74, 43.

Iben, I. 1967, Ap. J., 147, 624.

Johnson, H. L. 1966, Ann. Rev. of Astronomy and Astrophysics, Vol. 4, (Palo Alto, Calif., Annual Reviews, Inc.).

Johnson, H. L. and Sandage, A. R. 1955, Ap. J., 121, 616.

King, I. 1963, A. J., 68, 282.

Kruszewski, A. 1961, Acta Astronomica, Vol. II, No. 4.

Limber, D. N. 1960, Ap. J., 131, 168.

Meinel, A. B. and Schulte, D. H. 1967, Atlas of Grating Spectra, in preparation.

Morgan, W. W. 1959, P. A. S. P., 71, 92.

Morgan, W. W. and Mayall, N. U. 1957, P. A. S. P., 69, 291.

Morgan, W. W., Keenan, P. C., and Kellman, E. 1943, An Atlas of Stellar Spectra, (Chicago: Univ. of Chicago Press).

Öhman, Y. 1934, Ap. J., 80, 171.

Oort, J. H. 1940, Ap. J., 91, 273.

Pskovskii, Yu. P. 1965, Astr. Zu., 42, 323.

Roberts, M. S. 1956, A. J., 61, 195.

Salpeter, E. E. 1955, Ap. J., 121, 161.

Sandage, A. R. 1957a, Ap. J., 125, 422.

Sandage, A. R. 1957b, Ap. J., 126, 326.

Sandage, A. R. 1962a, Ap. J., 135, 333.

Sandage, A. R. 1962b, Ap. J., 135, 349.

Schwarzschild, M. 1954, A.J., 59, 273.

Schwarzschild, M., Schwarzschild, B., Searle, L., and Meltzer, A. 1957, Ap.J., 125, 123.

Spinrad, H. 1962, Ap.J., 135, 715.

Stebbins, J. and Whitford, A.E. 1948, Ap.J., 108, 413.

Tifft, W.G. 1961, A.J., 66, 390.

Tifft, W.G. 1963, A.J., 68, 302.

van den Bergh, S. 1957, Ap.J., 125, 445.

van den Bergh, S., and Henry, R.C. 1962, Publ. of the David Dunlap Obs., Vol. II, No. 10.

Westerlund, B. 1967, private communication.

Whipple, F.L. 1935, Harv. Coll. Obs. Circular, No. 404.

Whitford, A.E. 1964, I.A.U. Symp. No. 24.

Willstrop, R.V. 1965, Mem. of the R.A.S., Vol. 69, Part 3.

Wilson, O.C. 1959, Ap.J., 130, 496.